Adolescent neurostimulation of dopamine circuit reverses genetic deficits in frontal cortex function

Surjeet Mastwal[1#], Xinjian Li[1#], Rianne Stowell[2#], Matthew Manion[1], Wenyu Zhang[1,2], Nam-Shik Kim[3], Ki-jun Yoon[3], Hongjun Song[3], Guo-li Ming[3], Kuan Hong Wang[1,2*]

[1]Unit on Neural Circuits and Adaptive Behaviors, National Institute of Mental Health, Bethesda, MD 20892

[2]Department of Neuroscience, Del Monte Institute for Neuroscience, University of Rochester Medical Center, Rochester, NY 14642

[3]Department of Neuroscience, Mahoney Institute for Neurosciences, Perelman School of Medicine, University of Pennsylvania, Philadelphia, PA 19104

[#]These authors contributed equally to this work

*Correspondence: kuanhong_wang@urmc.rochester.edu

ABSTRACT

Dopamine system dysfunction is commonly implicated in adolescent-onset neuropsychiatric disorders. Although psychosis symptoms can be alleviated by antipsychotics, cognitive symptoms remain unresponsive to such pharmacological treatments and novel research paradigms investigating the circuit substrates underlying cognitive deficits are critically needed. The frontal cortex and its dopaminergic input from the midbrain are implicated in cognitive functions and undergo maturational changes during adolescence. Here, we used mice carrying mutations in the *Arc* or *DISC1* genes to model mesofrontal dopamine circuit deficiencies and test circuit-based neurostimulation strategies to restore cognitive functions. We found that in a memory-guided spatial navigation task, frontal cortical neurons were activated coordinately at the decision-making point in wild-type but not *Arc* mutant mice. Chemogenetic stimulation of midbrain dopamine neurons or optogenetic stimulation of frontal cortical dopamine axons in a limited adolescent period consistently reversed genetic defects in mesofrontal innervation, task-coordinated neuronal activity, and memory-guided decision-making at adulthood. Furthermore, adolescent stimulation of dopamine neurons also reversed the mesofrontal circuit and cognitive deficits in *DISC1* mutant mice. Our findings reveal common mesofrontal circuit alterations underlying the cognitive deficits caused by two different genes and demonstrate the feasibility of adolescent neurostimulation to reverse these circuit and behavioral deficits. These results may suggest developmental windows and circuit targets for treating cognitive deficits in neurodevelopmental disorders.

INTRODUCTION

Dysfunctions of the dopamine system are commonly implicated in neuropsychiatric disorders such as schizophrenia and substance-use disorders [1-3]. In addition, the treatment effect of antipsychotic medication is related to its effectiveness in blocking dopamine D2 receptors [4,5]. However, psychiatric symptoms include not only psychosis that can be treated by antipsychotics, but also cognitive disabilities in executive functions and memory [5-7]. While current antipsychotic therapies based on D2 antagonism have little effect on cognitive disabilities [7-10], frontal cortical dopamine deficits are reported in schizophrenia and the role of frontal cortical dopamine D1 receptor activation in cognitive function has been demonstrated in animal studies [11-14]. Unfortunately, due to safety and bioavailability issues, very few D1 receptor agonists have progressed to clinical testing [15-17]. The long-standing difficulty of developing effective pharmacological treatments for cognitive symptoms suggests the necessity of new investigative approaches, such as evaluating the underlying neural circuitry and its potential for modification.

Dopamine regulates a multitude of behavioral functions through different anatomical pathways from dopaminergic neurons in the midbrain ventral tegmental area (VTA) and substantia nigra to cortical and subcortical target regions [18-21]. The mesofrontal pathway innervates the frontal cortex and an optimal level of dopamine is important for normal frontal circuit functions [22-25]. The frontal cortical circuit integrates dopaminergic signals with multisensory and memory information to control behavioral actions [26-29]. Together, the frontal cortex and its dopaminergic input form a critical substrate for cognitive functions and a hypoactive frontal cortical dopamine system is found in schizophrenia patients [5,14]. Genetic disruptions of several genes involved in synaptic functions and related to psychiatric disorders, such as *Arc* and *DISC1* [30-33], lead to hypoactive

mesofrontal dopaminergic input in mice [34-36]. However, whether these genetic deficits in frontal cortex function can be reversed through therapeutic interventions remains unknown.

Adolescence is an important period for the development of cognitive control functions and exploration behaviors [37-39]. Cognitive control deficits often emerge during adolescence as a characteristic manifestation of several psychiatric disorders including schizophrenia and substance-use disorders [2,3,40]. Developmental studies of the mesofrontal dopamine projection in both non-human primates and rodents suggest that this pathway exhibits a protracted maturation through adolescence [41-45]. Importantly, the structure and function of the mesofrontal circuit are malleable to experience; activity-dependent modification during adolescence and adolescent exposure to substances of abuse can produce long-lasting deficits [46-49]. However, it is unknown whether adolescent intervention in this pathway can induce long-lasting circuit changes conducive for the recovery of cognitive function from genetic deficits.

Mouse genetic models of frontal dopamine deficits and the adolescence malleability of this circuit present opportunities to investigate the cellular substrates underlying cognitive deficits and test potential treatment strategies [34-36]. In this study, using single-cell resolution neuronal ensemble imaging in freely behaving animals, we identified a disruption of neuronal coordination in frontal cortex that is associated with cognitive impairment in mouse models. Furthermore, taking advantage of the activity-dependent adolescent plasticity in the mesofrontal circuit, we developed targeted chemogenetic and optogenetic neuromodulation techniques that are able to reverse the neural coordination and cognitive behavioral deficits in adult animals. Our results demonstrate the capability of adolescent frontal dopamine circuit stimulation to achieve long-term reversal of cognitive deficits and suggest potential translational targets and strategies for psychiatric treatments.

RESULTS

Characterization of cognitive and mesofrontal innervation deficits in *Arc* mutant mice

We first used an *Arc* mutant model of a hypo-functioning mesofrontal circuit [36] for behavioral, anatomical tracing and neural activity imaging studies. To assess whether genetic disruption of *Arc* (by knocking-in a GFP reporter cassette [50]) affects cognitive control of behavior, we examined wild-type and *Arc* homozygous mutant mice in a Y-maze spatial navigation task. This task takes advantage of the innate spatial navigation ability of mice and does not require extensive pretraining, making it well suited for both developmental and adult testing [51-53]. Wild-type mice explore the three arms of the maze using a memory-based decision-making strategy, preferring to visit a new arm instead of the most recently visited arm (Fig. 1a). The percentage of new arm visits out of the total arm visits is referred to as "alternation percentage", which is approximately 67% in wild-type mice and significantly above the chance level from random exploration (50%). By contrast, the alternation percentage in *Arc* mutant mice is significantly reduced towards the chance level ($p = 0.001$, t-test, $t(15) = 3.975$, *WT*: 67.2±2.6%, vs. *Arc*-/-: 53.4±2.3%, N = 8 and 9 mice, respectively; Fig. 1b). *Arc* mutant mice showed a similar number of total arm entries as the wild-type mice (Fig. 1c), suggesting that the *Arc* mutation did not affect overall locomotor activity or motivation level. Taken together, these results suggest that *Arc* mutant mice have a deficit in memory-guided choice behaviors.

Optimal performance in the Y-maze requires an intact frontal cortex and ventral tegmental area [54-56]. The M2 region of the frontal cortex plays an important role in action planning, generating the earliest neural signals related to upcoming choice during spatial navigation [57,58]. To verify the involvement of the M2 cortex in Y-maze alternation, we expressed the chemogenetic

inhibitor DREADD-Gi [59] in M2 with an Adeno-Associated Viral (AAV) vector and used Clozapine-N-Oxide (CNO) injection to inhibit M2 neural activity in wild-type mice (Supplementary Fig. 1a). We found that the alternation percentage was significantly reduced in the DREADD-Gi animals compared with control animals ($p = 0.017$, t-test, $t(10)=2.845$, Ctrl: 64.6±1.8%, Gi:54.1±3.2%, N=6 for each group, Supplementary Fig. 1b), while other aspects of motor behaviors in this task were not affected (Supplementary Fig. 1c and 1d). These results confirm the involvement of M2 frontal cortical neurons in memory-guided decision-making during the Y-maze task.

Dopaminergic input from the ventral tegmental areas is critical to optimal frontal cortical function in controlling cognitive processes [22-24]. We examined the anatomical structure of the frontal dopaminergic projection to determine if this input was altered in *Arc* mutant mice. A Tyrosine Hydroxylase (TH), rather than a Dopamine Transporter (DAT), transgenic Cre line was used to efficiently label mesofrontal dopamine neurons, because of the higher expression level of TH over DAT in these neurons [60,61]. Cre-dependent AAV vectors were injected into the VTA of *TH-Cre* mice to label dopaminergic axons with tdTomato and highlight boutons with synaptophysin-GFP (Fig. 1d and e) [46,62,63]. Although the dopaminergic axon length in the M2 frontal cortex (normalized by the number of labeled cells in VTA) was not significantly different between *Arc* mutant and wildtype animals (Fig. 1f), we found a significant reduction in the dopaminergic bouton density in this region in *Arc* mutant mice compared to wildtype animals ($p = 0.034$, t-test, $t(12)=2.393$, *WT*: 100±5%, *Arc* -/-:84±5%, N=7 for each group; bouton density normalized by axon length; Fig. 1g). These results suggest that dopaminergic innervations of the M2 frontal cortex are reduced in *Arc* mutant mice, which agrees with our previous findings of reduced frontal dopamine release and mesofrontal activity in *Arc-/-* mice [36]. Our new results

provide further anatomical evidence for a hypofunctional mesofrontal dopamine circuit in these mice.

Task-coordinated frontal neuronal ensemble activity is disrupted in *Arc* mutant mice

To determine how M2 neuronal activities during Y-maze performance might be affected by *Arc* mutation and reduced dopaminergic input, we expressed a genetically encoded calcium indicator GCaMP6 [64] in superficial layer (L2/3) M2 neurons and used a head-mounted miniaturized microscope [62,65-67] to image task-related neuronal ensemble activity in adult wild-type and *Arc*-/- mice (Fig. 2a). The microscope lens was placed above the pial surface rather than inserted into the cortex to avoid damage of M2 neurons, and neuronal activities in superficial cortical layers were imaged (Supplementary Fig. 2a-2c, Supplementary Movie 1). We found that the activity of individual M2 neurons occurred at various positions along the track during Y-maze navigation (Fig. 2b). An increased proportion of neurons showed peak activation when the wild-type animal was near the center of the maze before making an arm entry (Fig. 2c). In contrast, this proportion was significantly reduced in *Arc* mutant mice compared to wild type animals ($p < 0.0001$, chi-square test, *WT* 938 cells from 8 mice, *Arc*-/- 1338 cells from 7 mice). This effect is not due to a general reduction of neural activity in *Arc*-/- mice, because there is no difference between wild-type and *Arc*-/- mice in the average activity of neurons throughout the task period (Supplementary Fig. 2d-f). In addition, there is no correlation between the average activity of neurons with alteration behaviors in Y-maze (Supplementary Fig. 2j). Thus, these results suggest that the coordinated activation of M2 neurons before making a choice is disrupted in *Arc* mutant mice.

To further examine how exploratory choices may be encoded in the activities of individual M2 neurons, we compared the neuronal activity patterns along the navigation trajectories leading

to new arm visits versus old arm visits. Neurons selective for alternation were identified by differential neural activation between alternating and non-alternating paths (Fig. 2d). This analysis showed that the proportion of alternation-selective neurons increased in the wild type mice as the animal approached the maze center, but this increase was blunted in the *Arc* mutant animals ($p < 0.0001$, chi-square test, Fig. 2e). These same mutant animals also showed a specific reduction of alternation choices in the Y-maze ($p = 0.047$, t-test, $t(13)=2.196$, *WT*: 67.8 ± 4.4%, N = 8 mice; *Arc-/-*: 54.5 ± 4.1%, N = 7 mice, Supplementary Fig. 2g-i), replicating the deficit we observed in separate groups of animals that did not carry the miniaturized microscope (Fig. 1b). Together, these results demonstrate that both task-related frontal cortical activity and memory-guided decision behavior are impaired in *Arc* mutant mice.

Adolescent dopamine neuron stimulation leads to long-term reversal of mesofrontal circuit deficits

Given the hypo-functioning mesofrontal dopaminergic circuit in *Arc* mutant mice, we next investigated the possibility of developing neurostimulation strategies to restore normal circuit functions. We have previously shown that a brief stimulation of midbrain dopamine cells during adolescence, but not adult, leads to rapid formation of mesofrontal dopaminergic boutons and enhanced mesofrontal circuit activity in wild-type mice [46]. Here, we chose to test the long-term effect of this adolescent intervention strategy on the frontal circuit and memory-guided decision-making deficits in adult *Arc* mutant mice.

To stimulate dopamine neuron activity, we expressed chemogenetic activator DREADD-Gq [68] in the VTA dopamine cells using a combination of stereotaxically injected Cre-dependent AAV vectors and a *TH-Cre* transgenic mouse line [46] (Fig. 3a, Supplementary Fig. 3a). CNO (1mg/kg) was injected systemically to enhance the activity of DREADD-Gq-expressing dopamine

neurons. To control for any potential off-target effect of CNO, another group of *TH-Cre* mice that expressed AAV-mCherry reporter in dopamine neurons also received CNO injection.

Previous studies have shown that DREADD-Gq induced neural activation reaches its peak approximately 1 hr after CNO injection and returns to baseline approximately 9 hr after injection [68]. Increased VTA dopamine activity is known to enhance frontal cortical activity, which can be measured with calcium indicator GCaMP6 [36,46,69]. We validated the DREADD-Gq induced enhancement of mesofrontal activity by examining M2 cortical activity with GCaMP6 before and after CNO injection in these mice (Fig. 3a and b, Supplementary Fig. 3b). There was a significant increase in the M2 cortical activity measured 1 hr after the injection of CNO in DREADD-Gq animals, whereas no significant effect occurred in control mCherry animals (DREADD-Gq: 82±17% vs. mCherry Ctrl: 20±14%, $p = 0.018$, t-test, $t(10)=2.814$, N=6 for each group; Fig. 3c). In addition, saline injection in DREADD-Gq expressing mice did not alter M2 neural activity, and CNO-induced increase in M2 neural activity was suppressed by D1 antagonist SCH23390 (Supplementary Fig. 3c). These results confirmed CNO-induced activation of the mesofrontal dopaminergic circuit in DREADD-Gq animals.

After the validation of activity enhancement by chemogenetic stimulation of dopamine neurons, we examined if this treatment would have any long-term effect on the circuit deficits in *Arc* mutant mice. We first tested whether the structural deficits in the mesofrontal dopaminergic circuit would be affected by adolescent dopamine neuron stimulation. DREADD-Gq or mCherry expression was combined with tdTomato and synaptophysin-GFP to label dopaminergic axons and boutons in the *Arc* mutant animals (*Arc*-/-;*TH-Cre*). After three CNO treatments in adolescence (one injection per day for three days in mice 5 weeks of age in their home cages), the mice were kept in their regular home cage until adulthood (8 weeks) for histological assessment (Fig. 3d).

Although the mesofrontal dopamine axon length did not show any difference (Fig. 3e), we found a significant increase in dopaminergic bouton density in DREADD-Gq mice compared to control animals (Ctrl:100±4% vs. Gq:120±6%, $p = 0.013$, t-test, $t(18)=2.763$, N=10 for each group; Fig. 3f). These results suggest that adolescent dopamine neuron stimulation in *Arc* mutant mice led to a long-term enhancement of the connection between dopaminergic axons and M2 frontal cortical neurons, thereby ameliorating the structural deficits in these mice.

We next tested whether adolescent dopamine neuron stimulation would also lead to long-term improvement of the functional deficits in the mesofrontal circuit of *Arc* mutant mice. Our previous work indicated that *Arc* mutants have reduced frontal cortical response to VTA stimulation [36]. Using the same assay in adult mice, we found that the cortical calcium activity in response to VTA electrical stimulation was significantly enhanced in DREADD-Gq mice compared to control mCherry mice after adolescence CNO treatment (Fig. 3g-i). These results suggest that adolescent dopamine neuron stimulation also leads to long-term improvement of the functional deficits in the mesofrontal dopaminergic circuit of *Arc* mutants.

Adolescent dopamine neuron stimulation leads to restoration of coordinated frontal neuronal activity and cognition in adulthood

To further examine whether the uncoordinated frontal neural activity patterns in *Arc* mutant mice during the Y-maze task would be renormalized by this adolescent dopamine neuron stimulation strategy, we conducted calcium imaging using the head-mounted miniature microscope in these mice (Fig. 4a). We found that the coordinated activation of neurons near the maze center (Fig. 4b) and the proportion of alternation-selective neurons (Fig. 4c) were both significantly enhanced in *Arc* mutant mice that received the DREADD-Gq activation compared to the mCherry control group ($p < 0.0001$, chi-square tests, DREADD-Gq 1008 cells from 7 mice,

mCherry 1286 cells from 7 mice). In contrast, the average activity of M2 neurons throughout the task period was not affected by adolescent DREADD-Gq stimulation (Supplementary Fig. 4a-c). Strikingly, the DREADD-Gq stimulated animals also showed an enhancement of behavioral alternation ($p = 0.010$, t-test, $t(12)=3.043$, Ctrl:56.8±2.8%, Gq:67.6±2.2%, N=7 each group, Fig 4d), reaching a level comparable to that in the wild-type mice (Fig. 1b). Total arm entries were not affected (Fig. 4e), suggesting no alternations in general locomotor activity. These results indicate that adult task-related functional activity in the M2 frontal cortex is restored by adolescent dopamine neuron stimulation in *Arc* mutant mice.

Efficacy requirements for adolescent dopamine neuron stimulation

To further characterize the experimental conditions that are important for the restoration of memory-guided decision-making behavior in *Arc* mutant mice, we examined several variables including post-stimulation test interval, stimulation duration, and the age of stimulation. First, we replicated the effects of adolescent dopamine neuron stimulation on Y-maze navigation in adulthood in another cohort of *Arc* mutant mice ($p = 0.023$, t-test, $t(12)=2.598$, Ctrl:59.5±2.4%, Gq:68.5±2.5%, N=7 for each group) (Fig. 5a). Furthermore, when tested only one day after the three-day CNO treatment procedure (one injection per day) in adolescence, *Arc* mutant mice already showed an increased alternation percentage ($p = 0.031$, t-test, $t(20)=2.322$, Ctrl:55.8±2.9%, Gq:64.7±2.5%, N=11 for each group) (Fig. 5b), which is comparable to the effect observed one-month after treatment in adult mice (Fig. 5a). These results suggest that the adolescent neurostimulation effect on cognitive behavioral improvement is both fast acting and long lasting.

Second, we also tested a more intense CNO stimulation procedure involving two injections per day for three weeks (5 days per week) starting in adolescence. However, this strong three-

week stimulation did not enhance behavioral alternation and appeared to decrease it even further (Fig. 5c). These results indicate that excessive stimulation of dopamine neurons does not lead to functional improvement, consistent with previous studies showing that an optimal level of dopamine is important for normal cognitive function [22-24].

Third, we found that in adult *Arc* mutant mice with DREADD-Gq expression, three-day CNO injection did not lead to any effects on Y-maze alternation behavior assayed one-month later (Fig. 5d). These results indicate that adolescent, but not adult, intervention is critical for reversing this behavioral dysfunction, in agreement with the elevated adolescent structural and functional plasticity reported for the mesofrontal circuit [46]. In addition, because 3 weeks of adolescent CNO treatment or 3 days of adult CNO treatment in DREADD-Gq mice did not lead to any rescue effects, DREADD-Gq expression alone is unlikely to generate any behavior improvement. Taken together, our findings suggest that a brief stimulation of midbrain dopamine neurons in adolescence has a long-lasting effect to reverse the memory-guided decision-making deficits in *Arc* mutant mice, while not affecting other aspects of motor behaviors in the Y-maze (Supplementary Fig. 5).

Specific stimulation of adolescent frontal dopaminergic axons reverses both cognitive and psychomotor deficits

To further evaluate the impact of adolescent dopamine neuron stimulation on another frontal cortex-dependent behavioral deficit in *Arc* mutant mice, we subjected these mice to an amphetamine-induced hyperactivity test, which is considered an animal model for drug-induced psychomotor symptoms [36,70]. Classical neuropharmacological studies have shown that amphetamine-induced locomotor activity is facilitated by dopaminergic input to the nucleus accumbens but inhibited by dopaminergic input to the frontal cortex [71-73]. Consistent with a

hypoactive frontal dopamine input, *Arc* mutant mice showed hyper-reactivity to amphetamine compared to the wild-type mice (Figure Supplementary Fig. 6a) as reported before [36].

However, we found that adolescent stimulation of VTA dopamine neurons through DREADD-Gq did not reduce the hyper-reactivity to amphetamine in adult *Arc* mutant mice (Supplementary Fig. 6b). Dopamine neurons in the VTA include separate neuronal populations that project to the frontal cortex and the nucleus accumbens, respectively [18,61]. Our results suggest that adolescent stimulation of both populations of VTA neurons in mesofrontal and mesoaccumbens pathways, which have opposing effects on amphetamine-induced locomotor activity, result in no net change in this behavioral phenotype at adulthood.

Subsequently, we tested whether targeted stimulation of dopaminergic axons projecting to the frontal cortex would be a better strategy to reinstate memory-guided decision-making in the Y-maze task and prevent amphetamine hyper-reactivity in *Arc* mutant mice. Although CNO in principle could be injected directly into the frontal cortex to stimulate DREADD-Gq labeled dopaminergic axons, we found in preliminary experiments that repeated injections (three times) in adolescent brain led to tissue deformation and damage. Therefore, we turned to a less invasive optogenetic method to enhance the activity of labeled axons using Stabilized Step Function Opsins (SSFOs), which can increase neural excitability over a 30-min time scale in response to a two-sec pulse of light [74].

To validate the effect of SSFO-based stimulation, we expressed Cre-dependent SSFO in the midbrain dopamine neurons and stimulated their axonal projections in the M2 frontal cortex with blue light through a cranial window (Fig. 6a; Supplementary Fig. 6c-d). We monitored M2 neural activity using calcium reporter GCaMP6 before and 30 min after light activation. Similar to the DREADD-Gq mediated activity changes in the mesofrontal circuit, frontal cortical activity

was increased after light activation compared to before in SSFO animals, and this increase was significantly higher than the control EGFP animals that were also exposed to the light ($p = 0.001$, t-test, $t(8)=5.135$, Ctrl: 7.5±3.1%, SSFO: 46.7±6.9%, N=5 each group, Fig. 6b-c, Supplementary Fig. 6e). These results indicate that light stimulation of SSFO-labeled frontal dopamine axons can enhance the activity in the mesofrontal circuit.

To determine whether adolescent stimulation of mesofrontal dopamine axons would be sufficient to reinstate memory-guided decision-making in *Arc* mutant mice, we stimulated SSFO-labeled dopamine axons in the frontal cortex once per day for three days in adolescence (Fig. 6d). When tested either one day after light stimulation or one month after in adulthood, SSFO-labeled mice showed a significant increase in the Y-maze alternation percentage compared to control EGFP animals (Fig. 6e, 1 day after, $p = 0.028$, t-test, $t(15)=2.440$, Ctrl:58.4±1.4%, SSFO:66.5±3.2%; Fig. 6g, adulthood, $p = 0.015$, t-test, $t(15)=2.748$, Ctrl: 55.5±2.5%, SSFO: 66.7±3.3%; N = 9 for Ctrl, N = 8 for SSFO). On the other hand, total arm entries were not affected (Fig. 6f and 6h). These results suggest that similar to VTA dopamine neuron stimulation, projection-specific stimulation of dopaminergic axons in the frontal cortex is sufficient to restore memory-guided decision-making in *Arc* mutant animals.

Moreover, SSFO-mediated frontal dopamine axon stimulation in adolescence also significantly reduced the hyper-reactivity to amphetamine in adult *Arc* mutant mice (*$p = 0.037$, $F(1,14)=5.3$, Two-way ANOVA, N = 8 each, Fig 6i). Thus, adolescent stimulation of dopaminergic projections in the frontal cortex provides an effective strategy for reversing frontal dysfunctions in both memory-guided decision-making and psychostimulant reactivity.

Adolescent dopamine neuron stimulation reverses cognitive deficits in *DISC1* mutant mice

Finally, we sought to determine if this adolescent neurostimulation strategy would be applicable to another genetic model with a hypoactive mesofrontal circuit. Previous studies showed that knocking-down *DISC1* or overexpressing a dominant negative *DISC1* reduced mesofrontal dopaminergic innervation, dopamine release and cognitive dysfunction [34,35]. Using a *DISC1* mouse model that contains a knocked-in mutation identified from a subset of human patients [33,75], we first examined whether mesofrontal activity is also impaired in this model by imaging the calcium activity of M2 frontal cortex with two-photon microscopy in response to VTA stimulation (Fig. 7a). Our results showed a reduction of VTA-induced frontal cortical activity in *DISC1* mutants compared to wildtype animals (10 pulse $F(1,10)=16.5$, $^*p=0.002$, Two-way ANOVA, N=6 mice per group, Fig. 7b), indicating a mesofrontal hypofunction in this *DISC1* mutant line consistent with other *DISC1* models [34,35].

To further determine if our *DISC1* mutants have deficits in memory-guided decision-making, we conducted the Y-maze test and found reduced alternation in the *DISC1* mutants compared to the wildtype animals ($p = 0.044$, t-test, $t(18)=2.171$, *WT*:66.8±2.6%, *DISC1+/-*:58.9±2.5%, N=10 for each group; Fig. 7c). Thus, similar to *Arc* mutant mice, *DISC1* mutant mice also exhibit a hypofunctional mesofrontal circuit and impaired cognitive function.

We then tested whether the same adolescent neurostimulation strategy used in the *Arc* mutant mice would also reverse the cognitive deficits in *DISC1* mutants. Remarkably, we found that the alternation percentage in adult *DISC1* animals was significantly increased after adolescent neurostimulation ($p = 0.012$, t-test, $t(9)=3.139$, Ctrl:60.7±2.4%, N=5, Gq:69.3±1.5% N=6, Fig. 7d), reaching a level comparable to the wild-type mice. Other aspects of motor behaviors in the Y-maze were not affected (Supplementary Fig. 7). Taken together, these results suggest that

adolescent dopamine neuron stimulation is effective for long-term cognitive improvement in two different genetic models of mesofrontal hypofunction.

DISCUSSION

Fast-acting and long-lasting cognitive rescue by adolescent dopamine circuit stimulation

In this study, we have demonstrated a powerful role of adolescent dopaminergic input in inducing long-lasting circuit reorganization to reverse genetic deficits in frontal cortex function. Previous studies of dopamine function have focused on its transient neuromodulatory actions on neural dynamics or involvement in reinforcement learning [76-79]. Here, by examining the effect of dopamine neuron stimulation over a developmental time scale, we have identified both fast acting and persistent effect of adolescent dopamine neuron activity at neuroanatomical, neurophysiological, and behavioral levels. The cognitive dysfunction present in adolescent mutant mice is readily reversed one-day after neurostimulation and the restored performance level is maintained even one-month later at adulthood. Interestingly, the behavioral improvement afforded by dopamine neuron stimulation is observed when the intervention was introduced transiently during the adolescence period, but not adulthood, suggesting a sensitive and limited time window for plasticity-inducing therapeutic manipulations within mesofrontal dopamine circuits. These results may also stimulate future research to identify the molecular and cellular mechanisms controlling the adolescent plasticity window and explore the possibility and therapeutic potential of reopening plasticity in adulthood [46,80-82].

Cellular alterations in the mesofrontal circuit underlying cognitive dysfunction and rescue

Our examination across different mechanistic levels suggests a coherent picture in which increased dopamine neuron activity in adolescence leads to enhanced frontal dopaminergic innervation and cortical response to dopamine. Previous electrophysiological studies have suggested that dopamine can act on five different receptors expressed in both excitatory and inhibitory neurons to increase signal-to-noise ratio and temporal synchrony in network electrophysiological activity [25,78,79,83-86]. The neural activity deficit in *Arc-/-* mice is manifested in the task-coordinated neuronal activation at the decision-making point, but not in the average activity throughout the task. The uncoordinated neural activation pattern in *Arc-/-* mice may contribute to increased noise and decreased signal for decision-making, consistent with the hypodopaminergic cortical state in *Arc-/-* mice and the computational role of dopamine in enhancing the signal-to-noise ratio of neuronal ensemble activities[25,78,79,83-86]. After adolescent dopamine neuron stimulation, frontal dopaminergic innervation and cortical response to dopamine are enhanced, which help to restore task-coordinated neuronal activation in adult animals. As coordinated neuronal activity in frontal cortex is implicated in cognitive functions [87,88], the restoration of this activity may underlie the rescue of the cognitive behavioral deficit in *Arc* mutant mice. It is interesting to note that dopaminergic signaling can impact both excitatory and inhibitory neurons in the frontal cortex, and the local GABAergic inhibitory network undergoes major functional remodeling during adolescence[81]. The microcircuit mechanisms underlying adolescent dopamine neuron stimulation induced neuronal coordination changes will be an exciting direction for future research.

Reversal of cognitive deficits in independent genetic models

Our studies have shown that the mesofrontal dopamine circuit is a common target disrupted by mutations in *Arc* and *DISC1*, both implicated in neuropsychiatric disorders [30-33]. *Arc* and *DISC1*

have different protein interaction partners and function in distinct molecular pathways. *Arc* is best understood for its role in regulating the trafficking of excitatory neurotransmitter receptors at synapses, whereas *DISC1* has been shown to act as a scaffold protein to interact with multiple cytoskeletal proteins and synaptic molecules [89-92]. Dopamine-related deficits have been reported in multiple *Arc* and *DISC1* mutant lines or direct knockdown of these molecules [34-36,93-95], but the exact molecular mechanisms underlying these deficits and the varying severity in different models remain to be elucidated in future studies. Considering the widely reported roles of *Arc* and *DISC1* in regulating activity-dependent synaptic plasticity[96,97], mutations in these genes may compromise activity-dependent maturation of the mesofrontal dopaminergic circuit. In the two mouse lines we tested, both *Arc* and *DISC1* mutations lead to a hypoactive mesofrontal circuit and deficits in memory-guided decision-making behaviors. Our study demonstrates that the cognitive behavioral phenotypes arising from distinct genetic origins can be effectively rescued by the same neurostimulation strategy targeting a convergent mesofrontal circuit phenotype during a critical adolescent window.

Reversal of both cognitive and psychomotor deficits by targeting frontal dopamine projections

Our work reveals a specific circuit target for long-lasting restoration of cognitive control functions. Dopamine neurons projecting to the frontal cortex are located in the VTA but are distinct from those projecting to the nucleus accumbens [18,61]. Our initial chemogenetic neuromodulation strategies targeted most of the dopamine neurons in the VTA. While changes in the mesofrontal dopamine circuit were clearly induced, we cannot rule out other potential changes in the brain that might be also induced by such a targeting strategy and result in the lack of net effect related to amphetamine reactivity. The more refined optogenetic (SSFO) neurostimulation

method allowed us to specifically target the dopaminergic axons projecting to the frontal cortex. Enhancing their activity transiently in adolescence is sufficient to not only restore memory-guided decision making in the Y-maze task but also prevent hyper-reactivity to amphetamine. Thus, the mesofrontal dopaminergic circuit may provide an important therapeutic target to restore both cognitive control functions and prevent psychomotor symptoms. While this study focused on the M2 region of the frontal cortex because it generates the earliest neural signals related to upcoming choice during spatial navigation and is optically most accessible[57,58], the medial prefrontal regions (anterior cingulate, prelimbic and infralimbic) beneath M2 also receive dense dopaminergic innervation and can act in concert with M2 in decision making[98]. It will be interesting for future research to further dissect the effects of dopaminergic activation in specific frontal subregions.

Achieving fast-acting and enduring improvement of cognitive function while avoiding psychotic exacerbation has been a long-standing challenge for neuroscience and psychiatric research [2,6,7,99]. Our results suggest that adolescent frontal dopaminergic projections may provide an effective target. Developmentally guided and circuit-based intervention strategies that use clinical brain stimulation, local pharmacological application, or behavioral training methods [37,39,86,100] to engage the adolescent mesofrontal dopamine circuit may offer new routes to treat cognitive and behavior control disorders.

METHODS

Experimental Model and Subject Details

Arc-/- [50], *DISC1*+/- [75], and hemizygote *TH-Cre* transgenic [101] mice in the C57BL/6 strain were used in this study. *Arc*-/-;*TH-Cre* and *DISC1*+/-;*TH-Cre* lines were generated by in-house breeding. Mice were normally housed in groups of 2-5 animals. Estrous cycles are known to affect frontal dopamine activity [102,103] and the experiments in this study are limited to male mice of appropriate genotypes. It will be important for future studies to examine female mice at various estrous stages. Litter mates were randomly assigned into control or experimental groups. Behavioral tests were run blinded to the experimental conditions. Experimental protocols were approved by the National Institute of Mental Health Animal Care and Use Committee and the University Committee on Animal Resources (UCAR) at the University of Rochester Medical Center.

Method Details

Spontaneous alternation in the Y-maze

A three-arm plexiglass Y-maze (45cm length X 8cm width X 12cm height for each arm) was used to test spontaneous alternation. Animals were brought into the testing room at least 30min prior to the start of the session to acclimate to the room. Room lights were dimmed to ~10-15 lux. Animals were placed in the start arm facing away from the center. Recording of the session was started when the animal started to move toward the center and the animal was allowed to freely explore the y-maze for 8 minutes. The Y-maze was cleaned with 70% ethanol between animals.

Videos of the sessions were analyzed blindly offline. Arms were identified as A, B, C. Starting from the start arm, entry into each arm was recorded as a sequence of arm letters. Entry

was recorded if all four paws of the animal entered the arm. The number of alternating entries (Triplet sequences with non-repeating letters, e.g. ABC) and total entries (total number of letters) were counted. Alternation percentage was calculated as: (total alternating entries/(total entries-2)) X100.

Amphetamine induced locomotion

An animal was placed in an open field arena (50 cm x 50 cm x 25 cm) and monitored by video camera for 10 minutes. After that, d-amphetamine (1.5 mg/kg) was injected (i.p.), and the animal was monitored by video camera for another 60 min in the arena. Locomotion was automatically tracked using the animal's body position by the Limelight video tracking system (Actimetrics-Coulbourn Instruments).

Calcium imaging with head-mounted miniature microscope

WT and *Arc*-/- animals were prepared for surgery following previous published procedures [66,104,105]. Mice were anesthetized with Avertin (1.5% solution given at 0.01 ml/g, i.p.) and treated with dexamethasone (0.2 mg/kg, s.c.) and carprofen (5 mg/kg, s.c.) to prevent brain swelling and inflammation. A piece of skull (3.5 mm in diameter) in the frontal cortex was removed after high-speed dental drilling. AAV2/9 -Syn-GCaMP6s (3-5x10^{12} copies/ml, 0.6 µl per animal) was infused into M2 frontal cortex (Bregma, AP1.7, ML0.8) from the pial surface using a micro-syringe pump [66]. A 3-mm coverslip was used to seal the cranial window and the exposed scalp was sutured after cranial window surgery. 7-10 days later, the baseplate of a miniaturized integrated fluorescent microscope (Inscopix) was fixed on top of the coverslip. Animals were habituated to the attachment of the microscope (20 minutes per day for 4 days), then imaged during the spontaneous Y maze alternation task.

Calcium imaging was performed in freely moving mice using the head-attached microscope (LED power: 0.6 - 1.0 mW; camera resolution: 1440 x1080 pixels). Images were acquired at 30 Hz using nVista 2.0 (Inscopix). At the beginning of each imaging session, the protective cap of the previously implanted baseplate was removed, and the microscope was attached. The imaging field of view was 900 × 600 μm^2 at 0.65 μm/pixel resolution and the imaging depth was selected by adjusting the focus of the microscope until clear neuronal signals were observed in online ΔF/F calcium video. The focal plane was 150-250 μm below the lens. Mouse behavior was recorded with a video camera (Limelight), which was synchronized with calcium imaging using the trigger-out signal from nVista.

Calcium imaging videos were analyzed by using Mosaic software (Inscopix) and custom-written scripts in Matlab following published algorithms [106,107]. Raw videos were first down-sampled by four-fold along spatial dimensions to reduce file size and noise. The mean fluorescence intensity of each pixel during a recording session (8 min) was calculated as F0 and changes in pixel intensity at time t were expressed as (Ft - F0)/F0 or ΔF/F0. To extract active neuronal signals, principal component and independent component analysis (PCA-ICA) was applied to the spatial-temporal data matrices of ΔF/F0 using CellSort and fastICA toolboxes (These toolboxes are freely downloadable from Matlab central). This analysis decomposes a spatiotemporal data matrix into independent components based on the skewness of data distribution. Each component has a characteristic spatial filter over the imaged area and a corresponding temporal signal during the imaging period. The spatial filter and the temporal signal of each component were graphically displayed and inspected by human observers who were blind to the experimental conditions of each video. If the spatial filter for a component overlapped with the dark shadows casted by blood vessels in the F0 image, this component was likely contributed by blood flow and was therefore

rejected. In addition, since calcium signals show characteristic fast-rising and slow-decaying time course [64], the temporal skewness of calcium signals is expected to be positive and those components with skewness less than 1 were rejected [107]. For each selected component, the corresponding temporal signal of each neuron was calculated from the ΔF/F0 video by subtracting the median value of the background area (in a doughnut shape surrounding the target cell) from the average value of the cell soma area.

To identify periods of increased neuronal activity, we searched for the rising phase of each calcium event (peak ΔF/F0 > 3 standard deviation of baseline fluctuation), which has been shown closely associated with neuronal spiking activities [64]. The start of this rising phase is detected when the 1st derivative of ΔF/F0 (calculated in 200 ms moving window) rises above 0 and continues to increase above 5 standard deviation of baseline fluctuation, and the end of this rising phase is detected when the 1st derivative of ΔF/F0 falls below 0. The magnitude of the calcium event is calculated as the ΔF/F0 difference between the start and end of the event.

To measure an animal's movement in the Y-maze, the center of body mass was tracked in background-subtracted behavioral video using custom-written Matlab scripts. The animal's movement in Y-maze was divided into trials. Each trial began when the animal started moving away from the terminal of one arm and ended after it stopped at the terminal of another arm. To analyze neuronal activity changes along the Y-maze track, the animal's position in each trial was mapped into 20 equally divided location bins from one terminal to another. The calcium activity for each neuron in each trial was then averaged according to the binned position. To compare neuronal activity under different experimental conditions, the spatially averaged activities were further averaged across trials. The resulting traces from all detected cortical neurons were sorted based on their peak activation time and displayed in temporal raster plots. The proportion of

neurons that showed maximal activity at each binned location was then calculated. To measure the alternation selectivity of neurons, neuronal activity difference between alternating and non-alternating trials were calculated at each track position. If the difference at a particular position is higher than 2 standard deviations of the differences at all other positions, the activity was determined as alternation-selective at the designated position.

Frontal cortex inhibition and Y-maze testing

Animals were prepared for surgery following previous published procedures [66,104,105]**.** Mice were anesthetized with Avertin (1.5% solution given at 0.01 ml/g, i.p.). 0.7µl of AAV8-CaMKIIa-hM4D(Gi)-mCherry ($4x10^{12}$ copies/ml, UNC Vector Core) or AAV8-Syn-mCherry ($3x10^{12}$ copies/ml, Boston Children's Hospital Viral Core) was injected into the M2 frontal cortex (from bregma: AP 1.7, ML0.5, DV1.0mm) bilaterally. After 2 weeks, mCherry expressing controls were injected with CNO (3mg/kg) and Gi expressing animals were injected with either CNO (3mg/kg) or 0.9% saline control. Animals were run in the Y-maze 1 hr after the injections. After behavioral testing, animals were perfused and M2 frontal cortical expression was confirmed by confocal microscopy of brain sections.

Labeling and imaging of VTA dopaminergic neurons and projections to the frontal cortex

AAV2/9-phSyn1(S)-Flex-tdTomato-T2A-SynEGFP-WPRE ($4x10^{13}$ copies/ml, Boston Children's Hospital Viral Core, 0.5µl) and AAV9.CAG.Flex.tdTomato.WPRE.bGH ($9x10^{12}$ copies/ml, Penn Vector Core, 0.3µl) were mixed together and injected into the right hemisphere of the midbrain region (from bregma: AP -3.2, ML0.5, DV4.4mm) of *Arc*+/+;*TH-Cre* and *Arc*-/-;*TH-Cre* animals. Animals were allowed to recover for ~2 weeks. Animals were then perfused with 0.9% saline followed by 4% paraformaldehyde (PFA) and post-fixed overnight at 4°C. Coronal 100 µm thick sections in the frontal cortical and midbrain regions were prepared with a

sliding microtome. 3 sections in the frontal cortical region (AP 1.6, 1.8, and 2.0; 25x lens, 10 µm Z-stack, 10 stacks per section) and 5 sections in the midbrain region (AP -2.9, -3.1, -3.3, -3.5 and -3.7; 10x lens, single-frame images) were imaged in both the green and red channels using confocal microscopy (Olympus FV1000). For the frontal cortex, each image stack was maximum projected, and the 10 stacks were stitched together for each section. Animals that did not show VTA labeling were excluded from further analysis.

Image analysis was carried out using custom Matlab scripts. For boutons and axons, an ROI for the M2 region was drawn in each section using the mouse brain atlas (Paxinos) as reference, and boutons and axons were identified within this region. SypGFP labeled green channel images were used for bouton quantification. Boutons were detected automatically using a Laplacian filter and thresholded at 5 standard deviations above background. tdTomato labeled red channel images were used for the axon quantification. Axons were detected automatically using a Hessian filter, thresholded at 2 standard deviations above background, and skeletonized. For the midbrain sections, cells were detected automatically using a Laplacian filter and thresholded at 2 standard deviations above background. For each animal, the bouton density was normalized by the total axon length, and the total axon length was normalized by the total number of tdTomato labeled midbrain dopamine cells.

Expression of DREADD-Gq in midbrain dopamine neurons and validation of CNO-induced mesofrontal activation

0.7 µl of pAAV8-hSyn-DIO-hM3D(Gq)-mCherry ($6x10^{12}$ copies/ml, UNC Vector Core) or pAAV8-hSyn-DIO-mCherry ($3x10^{12}$ copies/ml, UNC Vector Core) was injected into the right hemisphere of the midbrain region (from bregma: AP -3.2, ML0.5, DV4.4mm) and 0.7µl of AAV1.Syn.Flex.GCaMP6s.WPRE.SV40 ($2x10^{12}$ copies /ml, Penn Vector Core) was injected into

the right hemisphere of the frontal cortex (from bregma: AP 1.7, ML 0.7, DV 0.4mm) of *TH-Cre* adult animals.

After ~2 weeks, a cranial window was opened above the AAV-GCaMP6 injected region in the frontal cortex (from Bregma: AP 1.0-3.0 mm, ML 0.3-1.3 mm, covering the M2 region) in animals anesthetized with isofluorane (~1.5%). The cranial window was filled with silicone gel, covered with a glass cover slip, and sealed with dental cement. A head plate was glued on the skull for fixation during imaging. The animals were then taken off the anesthesia and allowed to recover for ~1hr before imaging. A two-photon microscope (FV1000, Olympus) was used to image the brain under the cranial window (excitation laser: 900 nm) using a 20x water immersion lens (NA 0.95) in the head fixed awake animal. Animals were imaged before and 1hr after CNO (1mg/kg, ip) injection. After imaging, animals were perfused, and DREADD-Gq expression was confirmed in the midbrain regions. Animals that did not show VTA labeling were excluded from further analysis.

Images were analyzed using NIH ImageJ. Two 2-min movies of spontaneous activity before and after CNO were analyzed. The mean pixel intensity in each image frame of the movie was calculated as Ft. Baseline fluorescence (F0) was defined as the average of the fluorescent signals (Ft) in the time series. Changes in calcium signals ($\Delta F/F$) are calculated as (Ft-F0)/F0. The standard deviation of the ($\Delta F/F$) was used as a quantitative measure of overall cortical activity.

CNO stimulation of DREADD-Gq in midbrain dopamine neurons and behavior testing

Animals were prepared for surgery as above. 0.7 µl of pAAV8-hSyn-DIO-hM3D(Gq)-mCherry or pAAV8-hSyn-DIO-mCherry was bilaterally injected into the midbrain region (from bregma: AP -3.2, ML0.5, DV4.4mm) of *Arc*-/-;*TH-Cre* or *DISC1*+/-;*TH-Cre* animals within postnatal days P21-P25. CNO (1mg/kg, ip) was injected 1 time per day for three days into the

animals within postnatal days P35-P42. For one-day-after tests, animals were tested on the Y-maze 1 day after the last injection day. For adulthood tests, animals were tested at 2~3-month age on the Y-maze. Some of the adult animals were also tested for amphetamine induced locomotion as described above. After behavior testing, animals were perfused, and DREADD-Gq expression was confirmed in the ventral midbrain region. Animals that did not show VTA labeling were excluded from further analysis.

CNO stimulation of DREADD-Gq in midbrain dopamine neurons and in vivo imaging of cortical activity

Animals were prepared for surgery as described above. 0.7 µl of pAAV8-hSyn-DIO-hM3D(Gq)-mCherry or pAAV8-hSyn-DIO-mCherry was bilaterally injected into the midbrain region (from bregma: AP -3.2, ML0.5, DV4.4mm) of *Arc*-/-;*TH-Cre* animals within postnatal days P21-P25. CNO (1mg/kg, ip) was injected 1 time daily for three days into the animals for activation within postnatal days P35-P42. At adulthood, GCaMP6 labeling, cranial window opening, and imaging during Y-maze were carried out as described above. After an interval of at least 1 day after miniscope imaging, animals were used for VTA electrical stimulation coupled with in vivo two-photon imaging. A bipolar stimulation electrode was placed into the VTA (from bregma: AP -3.2, ML 0.5, and DV 4.5mm) and glued in place in animals anesthetized with isofluorane (~1.5%). A head plate was also glued on to the skull. The animals were then taken off the anesthesia and allowed to recover for ~1hr before imaging. Time series images lasting ~40s (115 frames at 0.351 s/frame) were taken for each stimulus train, with the VTA stimulus delivered at 20s after the start of imaging. Image analysis was carried out as described above. Baseline fluorescence (F0) was defined as the average of the fluorescent signals (Ft) in the first 15s of the time series. Changes in calcium signals (ΔF/F) are calculated as (Ft-F0)/F0. After imaging, animals were perfused, and

DREADD-Gq expression was confirmed in the midbrain regions. Animals that did not show VTA labeling were excluded from further analysis.

CNO stimulation of DREADD-Gq in midbrain dopamine neurons and imaging of mesofrontal axons and boutons

Animals were prepared for surgery as described above. A mixture of 0.4 µl of pAAV8-hSyn-DIO-hM3D(Gq)-mCherry or pAAV8-hSyn-DIO-mCherry 0.5 µl AAV2/9-phSyn1(S)-Flex-tdTomato-T2A-SynEGFP-WPRE and 0.3 µl AAV9.CAG.Flex.tdTomato.WPRE.bGH was injected into the midbrain region (from bregma: AP -3.2, ML0.5, DV4.4mm) of *Arc*-/-;*TH-Cre* animals within postnatal days P21-P25. The procedure was later modified with a 0.6 µl of pAAV8-hSyn-DIO-hM3D(Gq)-mCherry or pAAV8-hSyn-DIO-mCherry first and then immediately followed by an injection of a mixture of 0.5 µl AAV2/9-phSyn1(S)-Flex-tdTomato-T2A-SynEGFP-WPRE and 0.3 µl AAV9.CAG.Flex.tdTomato.WPRE.bGH. 12 animals from the first procedure and 8 animals from the latter procedure were pooled together for the analysis. CNO (1mg/kg, i.p.) was injected 1 time daily for three days into the animals within postnatal days P35-P42. At adulthood, animals were then perfused with 0.9% saline followed by 4% PFA and post-fixed overnight at 4°C. Coronal 100 µm thick sections in the frontal cortical and midbrain regions were prepared with a sliding microtome. 3 sections in the frontal cortical region (AP 1.6, 1.8, and 2.0) and 5 sections in the midbrain region (AP -2.9, -3.1, -3.3, -3.5 and -3.7) were imaged in both the green and red channels using confocal microscopy. Image analysis was carried out as described above.

SSFO expression in midbrain dopamine neurons and validation of cortical light activation

0.7 µl of pAAV9-EF1a-DIO-hChR2(C128S/D156A)-EYFP (titer $5x10^{13}$ copies/ml diluted 1:20 in PBS, Penn Vector Core) or AAV2/1.CAG.FLEX.EGFP.WPRE.bGH (titer $8x10^{12}$

copies/ml, Penn Vector Core) was injected into the midbrain region (from bregma: AP -3.2, ML0.5, DV4.4mm) and 0.7 µl of AAV1.Syn.Flex.GCaMP6s.WPRE.SV40 (titer $8x10^{12}$copies/ml, Penn Vector Core) was injected into the frontal cortex (from bregma: AP 1.7, ML0.7, DV 0.4mm) of *TH-Cre* adult animals.

After ~2 weeks, cranial window (from Bregma: AP 1.0-2.5 mm, ML 1mm) opening and two-photon imaging was carried out as described above. Animals were imaged before and 30min after light activation with an optical fiber (200 µm in diameter, Thor Labs) connected to a 473 nm solid-state laser diode (CrystaLaser) with ~10 mW output from the fiber. Three spots separated by around 200 µm anterior-posterior in the center of the window were activated with a 2s light pulse for each spot. After imaging, animals were perfused, and SSFO expression was confirmed in the midbrain regions. Images were analyzed as described above. 3-min times series images of spontaneous activity before and after CNO were analyzed. Baseline fluorescence (F0) was defined as the average of the fluorescent signals (Ft) in the time series. The standard deviation of the ($\Delta F/F$) was used as a quantitative measure of overall cortical activity.

Light activation of SSFO in frontal dopaminergic axons and behavioral testing

0.7 µl of pAAV9-EF1a-DIO hChR2(C128S/D156A)-EYFP or AAV2/1.CAG.FLEX. EGFP.WPRE.bGH was bilaterally injected into the midbrain region (from bregma: AP -3.2, ML0.5, DV4.4mm) of *Arc*-/-;*TH-Cre* animals within postnatal days P21-P25. Around postnatal days P35-P42, a cranial window was opened in above the frontal cortex (from Bregma: AP 1.0-2.5 mm, ML 1mm across both sides of the midline) in animals anesthetized with isofluorane (~1.5%). The cranial window was filled with silicone gel, covered with a glass cover slip, and sealed with dental cement. A head bar was glued on the skull for fixation during light activation. Animals were allowed to wake and recover for at least 2 hrs. Animals were then head fixed and an

optical fiber (200 μm in diameter, Thor Labs) connected to a 473 nm solid-state laser diode (CrystaLaser) with ~10 mW output from the fiber was used to deliver 2 s light pulses to the frontal cortex. Three spots separated by around 200 μm anterior posterior in the center of the window were activated in each hemisphere. The light activation was repeated for two more days. For one-day-after tests, animals were tested in the Y-maze 1 day after the last injection day. For adulthood tests, animals of 2~3-month age were first tested in the Y-maze, then tested for amphetamine induced locomotion as described above. After behavior testing, animals were perfused, and SSFO expression was confirmed in the midbrain regions. Animals that did not show VTA labeling were excluded from further analysis.

Quantification and statistical analysis

Statistical analyses were performed in Prism 9 or Matlab. No statistical methods were used to predetermine sample size. Sample sizes were chosen based on previous studies using similar techniques to determine biological effects [36,46,62,67]. Statistical differences between the means of two groups were evaluated with two-tailed *t*-test and normality was confirmed with Shapiro–Wilk test. Statistical differences between the means of multiple groups were determined using ANOVA. Statistical differences between two proportions were evaluated with chi-squared test.

Acknowledgments

The authors thank Drs. Y. Chudasama, F. Wang, Z. He for critical reading of the manuscript and J. Pulizzi for technical assistance. This work was supported by grants from National Institutes of Health (ZIAMH002897 and R01MH127737 to K.H.W., F32MH124298 to R.S., U19MH106434

and R35NS116843 to H.S., and R35NS097370 to G.L.M.) and Del Monte Institute for Neuroscience at University of Rochester (to K.H.W.)

Author contributions

K.H.W. conceived and supervised the study. S.M., X.L., R.S. and K.H.W. designed the experiments. S.M., X.L., R.S., M.C., and W.Z. conducted experiments. S.M., X.L., R.S. and K.H.W. analyzed data. N.K., K.Y., H.S. and G.M. generated and provided the *DISC1*+/- mouse line. S.M., X.L., R.S. and K.H.W. wrote the paper with inputs from all authors.

Author notes:

Current address: Ki-Jun Yoon, Department of Biological Sciences, Korea Advanced Institute of Science and Technology (KAIST), Daejeon 34141, Republic of Korea. Nam-Shik Kim, Cell Therapeutics (CTX) Inc., Daejeon 35220, Republic of Korea.

Competing interests

The authors declare no competing interests.

REFERENCES

1 Saha, S., Chant, D., Welham, J. & McGrath, J. A systematic review of the prevalence of schizophrenia. *PLoS Med* **2**, e141, doi:10.1371/journal.pmed.0020141 (2005).

2 Insel, T. R. Rethinking schizophrenia. *Nature* **468**, 187-193, doi:10.1038/nature09552 (2010).

3 Volkow, N. D. *et al*. The conception of the ABCD study: From substance use to a broad NIH collaboration. *Dev Cogn Neurosci* **32**, 4-7, doi:10.1016/j.dcn.2017.10.002 (2018).

4 Howes, O. D. & Kapur, S. The dopamine hypothesis of schizophrenia: version III--the final common pathway. *Schizophr Bull* **35**, 549-562, doi:10.1093/schbul/sbp006 (2009).

5 Weinstein, J. J. *et al*. Pathway-Specific Dopamine Abnormalities in Schizophrenia. *Biol Psychiatry* **81**, 31-42, doi:10.1016/j.biopsych.2016.03.2104 (2017).

6 Green, M. F. Stimulating the development of drug treatments to improve cognition in schizophrenia. *Annu Rev Clin Psychol* **3**, 159-180, doi:10.1146/annurev.clinpsy.3.022806.091529 (2007).

7 Miyamoto, S., Duncan, G. E., Marx, C. E. & Lieberman, J. A. Treatments for schizophrenia: a critical review of pharmacology and mechanisms of action of antipsychotic drugs. *Mol Psychiatry* **10**, 79-104, doi:10.1038/sj.mp.4001556 (2005).

8 Davidson, M. *et al*. Cognitive effects of antipsychotic drugs in first-episode schizophrenia and schizophreniform disorder: a randomized, open-label clinical trial (EUFEST). *Am J Psychiatry* **166**, 675-682, doi:10.1176/appi.ajp.2008.08060806 (2009).

9 Keefe, R. S. *et al*. Comparative effect of atypical and conventional antipsychotic drugs on neurocognition in first-episode psychosis: a randomized, double-blind trial of olanzapine versus low doses of haloperidol. *Am J Psychiatry* **161**, 985-995, doi:10.1176/appi.ajp.161.6.985 (2004).

10 Barbui, C., Signoretti, A., Mule, S., Boso, M. & Cipriani, A. Does the addition of a second antipsychotic drug improve clozapine treatment? *Schizophr Bull* **35**, 458-468, doi:10.1093/schbul/sbn030 (2009).

11 Arnsten, A. F. Catecholamine regulation of the prefrontal cortex. *J Psychopharmacol* **11**, 151-162, doi:10.1177/026988119701100208 (1997).

12 Vijayraghavan, S., Wang, M., Birnbaum, S. G., Williams, G. V. & Arnsten, A. F. Inverted-U dopamine D1 receptor actions on prefrontal neurons engaged in working memory. *Nat Neurosci* **10**, 376-384, doi:10.1038/nn1846 (2007).

13 Castner, S. A., Williams, G. V. & Goldman-Rakic, P. S. Reversal of antipsychotic-induced working memory deficits by short-term dopamine D1 receptor stimulation. *Science* **287**, 2020-2022, doi:10.1126/science.287.5460.2020 (2000).

14 Slifstein, M. *et al*. Deficits in prefrontal cortical and extrastriatal dopamine release in schizophrenia: a positron emission tomographic functional magnetic resonance imaging study. *JAMA Psychiatry* **72**, 316-324, doi:10.1001/jamapsychiatry.2014.2414 (2015).

15 Girgis, R. R. *et al*. A proof-of-concept, randomized controlled trial of DAR-0100A, a dopamine-1 receptor agonist, for cognitive enhancement in schizophrenia. *J Psychopharmacol* **30**, 428-435, doi:10.1177/0269881116636120 (2016).

16 Marder, S. R. The NIMH-MATRICS project for developing cognition-enhancing agents for schizophrenia. *Dialogues Clin Neurosci* **8**, 109-113, doi:10.31887/DCNS.2006.8.1/smarder (2006).

17 Tamminga, C. A. The neurobiology of cognition in schizophrenia. *J Clin Psychiatry* **67**, e11 (2006).
18 Bjorklund, A. & Dunnett, S. B. Dopamine neuron systems in the brain: an update. *Trends in neurosciences* **30**, 194-202, doi:10.1016/j.tins.2007.03.006 (2007).
19 Beier, K. T. *et al*. Circuit Architecture of VTA Dopamine Neurons Revealed by Systematic Input-Output Mapping. *Cell* **162**, 622-634, doi:10.1016/j.cell.2015.07.015 (2015).
20 Lerner, T. N. *et al*. Intact-Brain Analyses Reveal Distinct Information Carried by SNc Dopamine Subcircuits. *Cell* **162**, 635-647, doi:10.1016/j.cell.2015.07.014 (2015).
21 Watabe-Uchida, M., Zhu, L., Ogawa, S. K., Vamanrao, A. & Uchida, N. Whole-brain mapping of direct inputs to midbrain dopamine neurons. *Neuron* **74**, 858-873, doi:10.1016/j.neuron.2012.03.017 (2012).
22 Arnsten, A. F., Cai, J. X., Murphy, B. L. & Goldman-Rakic, P. S. Dopamine D1 receptor mechanisms in the cognitive performance of young adult and aged monkeys. *Psychopharmacology (Berl)* **116**, 143-151, doi:10.1007/BF02245056 (1994).
23 Robbins, T. W. Chemical neuromodulation of frontal-executive functions in humans and other animals. *Exp Brain Res* **133**, 130-138, doi:10.1007/s002210000407 (2000).
24 Floresco, S. B. Prefrontal dopamine and behavioral flexibility: shifting from an "inverted-U" toward a family of functions. *Front Neurosci* **7**, 62, doi:10.3389/fnins.2013.00062 (2013).
25 Vander Weele, C. M. *et al*. Dopamine enhances signal-to-noise ratio in cortical-brainstem encoding of aversive stimuli. *Nature* **563**, 397-401, doi:10.1038/s41586-018-0682-1 (2018).
26 Fuster, J. M. *The prefrontal cortex*. 4th edn, (Academic Press/Elsevier, 2008).
27 Miller, E. K. & Cohen, J. D. An integrative theory of prefrontal cortex function. *Annu Rev Neurosci* **24**, 167-202, doi:10.1146/annurev.neuro.24.1.167 (2001).
28 Rushworth, M. F., Kolling, N., Sallet, J. & Mars, R. B. Valuation and decision-making in frontal cortex: one or many serial or parallel systems? *Curr Opin Neurobiol* **22**, 946-955, doi:10.1016/j.conb.2012.04.011 (2012).
29 Dalley, J. W., Cardinal, R. N. & Robbins, T. W. Prefrontal executive and cognitive functions in rodents: neural and neurochemical substrates. *Neurosci Biobehav Rev* **28**, 771-784, doi:10.1016/j.neubiorev.2004.09.006 (2004).
30 Purcell, S. M. *et al*. A polygenic burden of rare disruptive mutations in schizophrenia. *Nature* **506**, 185-190, doi:10.1038/nature12975 (2014).
31 Fromer, M. *et al*. De novo mutations in schizophrenia implicate synaptic networks. *Nature* **506**, 179-184, doi:10.1038/nature12929 (2014).
32 Thomson, P. A. *et al*. DISC1 genetics, biology and psychiatric illness. *Front Biol (Beijing)* **8**, 1-31, doi:10.1007/s11515-012-1254-7 (2013).
33 Wen, Z. *et al*. Synaptic dysregulation in a human iPS cell model of mental disorders. *Nature* **515**, 414-418, doi:10.1038/nature13716 (2014).
34 Niwa, M. *et al*. Knockdown of DISC1 by in utero gene transfer disturbs postnatal dopaminergic maturation in the frontal cortex and leads to adult behavioral deficits. *Neuron* **65**, 480-489, doi:10.1016/j.neuron.2010.01.019 (2010).
35 Niwa, M. *et al*. Adolescent stress-induced epigenetic control of dopaminergic neurons via glucocorticoids. *Science* **339**, 335-339, doi:10.1126/science.1226931 (2013).

36 Manago, F. *et al*. Genetic Disruption of Arc/Arg3.1 in Mice Causes Alterations in Dopamine and Neurobehavioral Phenotypes Related to Schizophrenia. *Cell Rep* **16**, 2116-2128, doi:10.1016/j.celrep.2016.07.044 (2016).
37 Dahl, R. E., Allen, N. B., Wilbrecht, L. & Suleiman, A. B. Importance of investing in adolescence from a developmental science perspective. *Nature* **554**, 441-450, doi:10.1038/nature25770 (2018).
38 Spear, L. P. Rewards, aversions and affect in adolescence: emerging convergences across laboratory animal and human data. *Dev Cogn Neurosci* **1**, 392-400, doi:10.1016/j.dcn.2011.08.001 (2011).
39 Larsen, B. & Luna, B. Adolescence as a neurobiological critical period for the development of higher-order cognition. *Neurosci Biobehav Rev* **94**, 179-195, doi:10.1016/j.neubiorev.2018.09.005 (2018).
40 Paus, T., Keshavan, M. & Giedd, J. N. Why do many psychiatric disorders emerge during adolescence? *Nat Rev Neurosci* **9**, 947-957, doi:10.1038/nrn2513 (2008).
41 Kalsbeek, A., Voorn, P., Buijs, R. M., Pool, C. W. & Uylings, H. B. Development of the dopaminergic innervation in the prefrontal cortex of the rat. *The Journal of comparative neurology* **269**, 58-72, doi:10.1002/cne.902690105 (1988).
42 Rosenberg, D. R. & Lewis, D. A. Postnatal maturation of the dopaminergic innervation of monkey prefrontal and motor cortices: a tyrosine hydroxylase immunohistochemical analysis. *The Journal of comparative neurology* **358**, 383-400, doi:10.1002/cne.903580306 (1995).
43 Naneix, F., Marchand, A. R., Pichon, A., Pape, J. R. & Coutureau, E. Adolescent stimulation of D2 receptors alters the maturation of dopamine-dependent goal-directed behavior. *Neuropsychopharmacology : official publication of the American College of Neuropsychopharmacology* **38**, 1566-1574, doi:10.1038/npp.2013.55 (2013).
44 Lambe, E. K., Krimer, L. S. & Goldman-Rakic, P. S. Differential postnatal development of catecholamine and serotonin inputs to identified neurons in prefrontal cortex of rhesus monkey. *The Journal of neuroscience : the official journal of the Society for Neuroscience* **20**, 8780-8787, doi:10.1523/JNEUROSCI.20-23-08780.2000 (2000).
45 Ye, Y. *et al*. Dopamine is Required for Activity-Dependent Amplification of Arc mRNA in Developing Postnatal Frontal Cortex. *Cereb Cortex* **27**, 3600-3608, doi:10.1093/cercor/bhw181 (2017).
46 Mastwal, S. *et al*. Phasic dopamine neuron activity elicits unique mesofrontal plasticity in adolescence. *The Journal of neuroscience : the official journal of the Society for Neuroscience* **34**, 9484-9496, doi:10.1523/JNEUROSCI.1114-14.2014 (2014).
47 Reynolds, L. M. *et al*. Early Adolescence is a Critical Period for the Maturation of Inhibitory Behavior. *Cerebral Cortex* (2018).
48 Jobson, C. L. *et al*. Adolescent Nicotine Exposure Induces Dysregulation of Mesocorticolimbic Activity States and Depressive and Anxiety-like Prefrontal Cortical Molecular Phenotypes Persisting into Adulthood. *Cerebral Cortex* (2018).
49 Walker, D. M. *et al*. Adolescence and Reward: Making Sense of Neural and Behavioral Changes Amid the Chaos. *The Journal of neuroscience : the official journal of the Society for Neuroscience* **37**, 10855-10866, doi:10.1523/JNEUROSCI.1834-17.2017 (2017).

50 Wang, K. H. *et al*. In vivo two-photon imaging reveals a role of arc in enhancing orientation specificity in visual cortex. *Cell* **126**, 389-402, doi:10.1016/j.cell.2006.06.038 (2006).
51 Lalonde, R. The neurobiological basis of spontaneous alternation. *Neurosci Biobehav Rev* **26**, 91-104, doi:10.1016/s0149-7634(01)00041-0 (2002).
52 Richman, C. L., Dember, W. N. & Kim, P. Spontaneous alternation behavior in animals: A review. *Current Psychological Research & Reviews* **5**, 358-391, doi:10.1007/bf02686603 (1986).
53 Belforte, J. E. *et al*. Postnatal NMDA receptor ablation in corticolimbic interneurons confers schizophrenia-like phenotypes. *Nat Neurosci* **13**, 76-83, doi:10.1038/nn.2447 (2010).
54 Pioli, E. Y. *et al*. Differential behavioral effects of partial bilateral lesions of ventral tegmental area or substantia nigra pars compacta in rats. *Neuroscience* **153**, 1213-1224, doi:10.1016/j.neuroscience.2008.01.084 (2008).
55 Delatour, B. & Gisquet-Verrier, P. Prelimbic cortex specific lesions disrupt delayed-variable response tasks in the rat. *Behav Neurosci* **110**, 1282-1298, doi:10.1037//0735-7044.110.6.1282 (1996).
56 Divac, I., Wikmark, R. & Gade, A. Spontaneous alternation in rats with lesions in the frontal lobes: an extension of the frontal lobe syndrome. *Physiological Psychology* **3**, 39-42 (1975).
57 Sul, J. H., Jo, S., Lee, D. & Jung, M. W. Role of rodent secondary motor cortex in value-based action selection. *Nat Neurosci* **14**, 1202-1208, doi:10.1038/nn.2881 (2011).
58 Sul, J. H., Kim, H., Huh, N., Lee, D. & Jung, M. W. Distinct roles of rodent orbitofrontal and medial prefrontal cortex in decision making. *Neuron* **66**, 449-460, doi:10.1016/j.neuron.2010.03.033 (2010).
59 Roth, B. L. DREADDs for Neuroscientists. *Neuron* **89**, 683-694, doi:10.1016/j.neuron.2016.01.040 (2016).
60 Sesack, S. R., Hawrylak, V. A., Matus, C., Guido, M. A. & Levey, A. I. Dopamine axon varicosities in the prelimbic division of the rat prefrontal cortex exhibit sparse immunoreactivity for the dopamine transporter. *The Journal of neuroscience : the official journal of the Society for Neuroscience* **18**, 2697-2708, doi:10.1523/JNEUROSCI.18-07-02697.1998 (1998).
61 Lammel, S. *et al*. Unique properties of mesoprefrontal neurons within a dual mesocorticolimbic dopamine system. *Neuron* **57**, 760-773, doi:10.1016/j.neuron.2008.01.022 (2008).
62 Wang, X. *et al*. Deconstruction of Corticospinal Circuits for Goal-Directed Motor Skills. *Cell* **171**, 440-455 e414, doi:10.1016/j.cell.2017.08.014 (2017).
63 Manion, M. T. C., Glasper, E. R. & Wang, K. H. A sex difference in mouse dopaminergic projections from the midbrain to basolateral amygdala. *Biol Sex Differ* **13**, 75, doi:10.1186/s13293-022-00486-4 (2022).
64 Chen, T. W. *et al*. Ultrasensitive fluorescent proteins for imaging neuronal activity. *Nature* **499**, 295-300, doi:10.1038/nature12354 (2013).
65 Ghosh, K. K. *et al*. Miniaturized integration of a fluorescence microscope. *Nat Methods* **8**, 871-878, doi:10.1038/nmeth.1694 (2011).

66 Li, X. *et al*. Skin suturing and cortical surface viral infusion improves imaging of neuronal ensemble activity with head-mounted miniature microscopes. *J Neurosci Methods* **291**, 238-248, doi:10.1016/j.jneumeth.2017.08.016 (2017).
67 Liu, Y. *et al*. Touch and tactile neuropathic pain sensitivity are set by corticospinal projections. *Nature* **561**, 547-550, doi:10.1038/s41586-018-0515-2 (2018).
68 Alexander, G. M. *et al*. Remote control of neuronal activity in transgenic mice expressing evolved G protein-coupled receptors. *Neuron* **63**, 27-39, doi:10.1016/j.neuron.2009.06.014 (2009).
69 Lavin, A. *et al*. Mesocortical dopamine neurons operate in distinct temporal domains using multimodal signaling. *The Journal of neuroscience : the official journal of the Society for Neuroscience* **25**, 5013-5023, doi:10.1523/JNEUROSCI.0557-05.2005 (2005).
70 Forrest, A. D., Coto, C. A. & Siegel, S. J. Animal Models of Psychosis: Current State and Future Directions. *Curr Behav Neurosci Rep* **1**, 100-116, doi:10.1007/s40473-014-0013-2 (2014).
71 Tzschentke, T. M. Pharmacology and behavioral pharmacology of the mesocortical dopamine system. *Progress in neurobiology* **63**, 241-320, doi:10.1016/s0301-0082(00)00033-2 (2001).
72 Chambers, R. A., Taylor, J. R. & Potenza, M. N. Developmental neurocircuitry of motivation in adolescence: a critical period of addiction vulnerability. *Am J Psychiatry* **160**, 1041-1052, doi:10.1176/appi.ajp.160.6.1041 (2003).
73 Le Moal, M. & Simon, H. Mesocorticolimbic dopaminergic network: functional and regulatory roles. *Physiological reviews* **71**, 155-234, doi:10.1152/physrev.1991.71.1.155 (1991).
74 Yizhar, O. *et al*. Neocortical excitation/inhibition balance in information processing and social dysfunction. *Nature* **477**, 171-178, doi:10.1038/nature10360 (2011).
75 Kim, N.-S. *et al*. Pharmacological rescue in patient iPSC and mouse models with a rare DISC1 mutation. *Nature communications* **12**, 1-11 (2021).
76 Tritsch, N. X. & Sabatini, B. L. Dopaminergic modulation of synaptic transmission in cortex and striatum. *Neuron* **76**, 33-50, doi:10.1016/j.neuron.2012.09.023 (2012).
77 Schultz, W. Multiple dopamine functions at different time courses. *Annu Rev Neurosci* **30**, 259-288, doi:10.1146/annurev.neuro.28.061604.135722 (2007).
78 Seamans, J. K. & Yang, C. R. The principal features and mechanisms of dopamine modulation in the prefrontal cortex. *Progress in neurobiology* **74**, 1-58, doi:10.1016/j.pneurobio.2004.05.006 (2004).
79 Lohani, S., Martig, A. K., Deisseroth, K., Witten, I. B. & Moghaddam, B. Dopamine Modulation of Prefrontal Cortex Activity Is Manifold and Operates at Multiple Temporal and Spatial Scales. *Cell Rep* **27**, 99-114 e116, doi:10.1016/j.celrep.2019.03.012 (2019).
80 Hoops, D. & Flores, C. Making Dopamine Connections in Adolescence. *Trends in neurosciences* **40**, 709-719, doi:10.1016/j.tins.2017.09.004 (2017).
81 Caballero, A. & Tseng, K. Y. GABAergic Function as a Limiting Factor for Prefrontal Maturation during Adolescence. *Trends in neurosciences* **39**, 441-448, doi:10.1016/j.tins.2016.04.010 (2016).
82 Mastwal, S., Cao, V. & Wang, K. H. Genetic Feedback Regulation of Frontal Cortical Neuronal Ensembles Through Activity-Dependent Arc Expression and Dopaminergic

Input. *Frontiers in Neural Circuits* **10**, 100, doi:ARTN 100 10.3389/fncir.2016.00100 (2016).
83 O'Donnell, P. Adolescent onset of cortical disinhibition in schizophrenia: insights from animal models. *Schizophr Bull* **37**, 484-492, doi:10.1093/schbul/sbr028 (2011).
84 Rolls, E. T., Loh, M., Deco, G. & Winterer, G. Computational models of schizophrenia and dopamine modulation in the prefrontal cortex. *Nat Rev Neurosci* **9**, 696-709, doi:10.1038/nrn2462 (2008).
85 Tseng, K. Y. & O'Donnell, P. Dopamine modulation of prefrontal cortical interneurons changes during adolescence. *Cereb Cortex* **17**, 1235-1240, doi:10.1093/cercor/bhl034 (2007).
86 Mukherjee, A., Carvalho, F., Eliez, S. & Caroni, P. Long-Lasting Rescue of Network and Cognitive Dysfunction in a Genetic Schizophrenia Model. *Cell* **178**, 1387-1402 e1314, doi:10.1016/j.cell.2019.07.023 (2019).
87 Sigurdsson, T., Stark, K. L., Karayiorgou, M., Gogos, J. A. & Gordon, J. A. Impaired hippocampal-prefrontal synchrony in a genetic mouse model of schizophrenia. *Nature* **464**, 763-767, doi:10.1038/nature08855 (2010).
88 Ito, H. T., Zhang, S. J., Witter, M. P., Moser, E. I. & Moser, M. B. A prefrontal-thalamo-hippocampal circuit for goal-directed spatial navigation. *Nature* **522**, 50-55, doi:10.1038/nature14396 (2015).
89 Zhang, W. *et al*. Structural basis of arc binding to synaptic proteins: implications for cognitive disease. *Neuron* **86**, 490-500, doi:10.1016/j.neuron.2015.03.030 (2015).
90 Kirov, G. *et al*. De novo CNV analysis implicates specific abnormalities of postsynaptic signalling complexes in the pathogenesis of schizophrenia. *Mol Psychiatry* **17**, 142-153, doi:10.1038/mp.2011.154 (2012).
91 Ishizuka, K., Paek, M., Kamiya, A. & Sawa, A. A review of Disrupted-In-Schizophrenia-1 (DISC1): neurodevelopment, cognition, and mental conditions. *Biol Psychiatry* **59**, 1189-1197, doi:10.1016/j.biopsych.2006.03.065 (2006).
92 El-Boustani, S. *et al*. Locally coordinated synaptic plasticity of visual cortex neurons in vivo. *Science* **360**, 1349-1354, doi:10.1126/science.aao0862 (2018).
93 Penrod, R. D. *et al*. Activity-regulated cytoskeleton-associated protein (Arc/Arg3.1) regulates anxiety- and novelty-related behaviors. *Genes Brain Behav* **18**, e12561, doi:10.1111/gbb.12561 (2019).
94 Salery, M. *et al*. Activity-Regulated Cytoskeleton-Associated Protein Accumulates in the Nucleus in Response to Cocaine and Acts as a Brake on Chromatin Remodeling and Long-Term Behavioral Alterations. *Biol Psychiatry* **81**, 573-584, doi:10.1016/j.biopsych.2016.05.025 (2017).
95 Gao, X. *et al*. Disturbed Prefrontal Cortex Activity in the Absence of Schizophrenia-Like Behavioral Dysfunction in Arc/Arg3.1 Deficient Mice. *The Journal of neuroscience : the official journal of the Society for Neuroscience* **39**, 8149-8163, doi:10.1523/JNEUROSCI.0623-19.2019 (2019).
96 Tropea, D., Hardingham, N., Millar, K. & Fox, K. Mechanisms underlying the role of DISC1 in synaptic plasticity. *J Physiol* **596**, 2747-2771, doi:10.1113/JP274330 (2018).
97 Shepherd, J. D. & Bear, M. F. New views of Arc, a master regulator of synaptic plasticity. *Nat Neurosci* **14**, 279-284, doi:10.1038/nn.2708 (2011).
98 Barthas, F. & Kwan, A. C. Secondary motor cortex: where 'sensory'meets 'motor'in the rodent frontal cortex. *Trends in neurosciences* **40**, 181-193 (2017).

99 Goff, D. C., Hill, M. & Barch, D. The treatment of cognitive impairment in schizophrenia. *Pharmacol Biochem Behav* **99**, 245-253, doi:10.1016/j.pbb.2010.11.009 (2011).

100 Luscher, C., Pascoli, V. & Creed, M. Optogenetic dissection of neural circuitry: from synaptic causalities to blue prints for novel treatments of behavioral diseases. *Curr Opin Neurobiol* **35**, 95-100, doi:10.1016/j.conb.2015.07.005 (2015).

101 Gong, S. *et al*. Targeting Cre recombinase to specific neuron populations with bacterial artificial chromosome constructs. *The Journal of neuroscience : the official journal of the Society for Neuroscience* **27**, 9817-9823, doi:10.1523/JNEUROSCI.2707-07.2007 (2007).

102 Becker, J. B. & Cha, J. H. Estrous cycle-dependent variation in amphetamine-induced behaviors and striatal dopamine release assessed with microdialysis. *Behav Brain Res* **35**, 117-125, doi:10.1016/s0166-4328(89)80112-3 (1989).

103 Dazzi, L. *et al*. Estrous cycle-dependent changes in basal and ethanol-induced activity of cortical dopaminergic neurons in the rat. *Neuropsychopharmacology : official publication of the American College of Neuropsychopharmacology* **32**, 892-901, doi:10.1038/sj.npp.1301150 (2007).

104 Cao, V. Y. *et al*. In vivo two-photon imaging of experience-dependent molecular changes in cortical neurons. *J Vis Exp*, doi:10.3791/50148 (2013).

105 Cao, V. Y. *et al*. Motor Learning Consolidates Arc-Expressing Neuronal Ensembles in Secondary Motor Cortex. *Neuron* **86**, 1385-1392, doi:10.1016/j.neuron.2015.05.022 (2015).

106 Hyvarinen, A. & Oja, E. Independent component analysis: algorithms and applications. *Neural Networks* **13**, 411-430, doi:10.1016/s0893-6080(00)00026-5 (2000).

107 Mukamel, E. A., Nimmerjahn, A. & Schnitzer, M. J. Automated analysis of cellular signals from large-scale calcium imaging data. *Neuron* **63**, 747-760, doi:10.1016/j.neuron.2009.08.009 (2009).

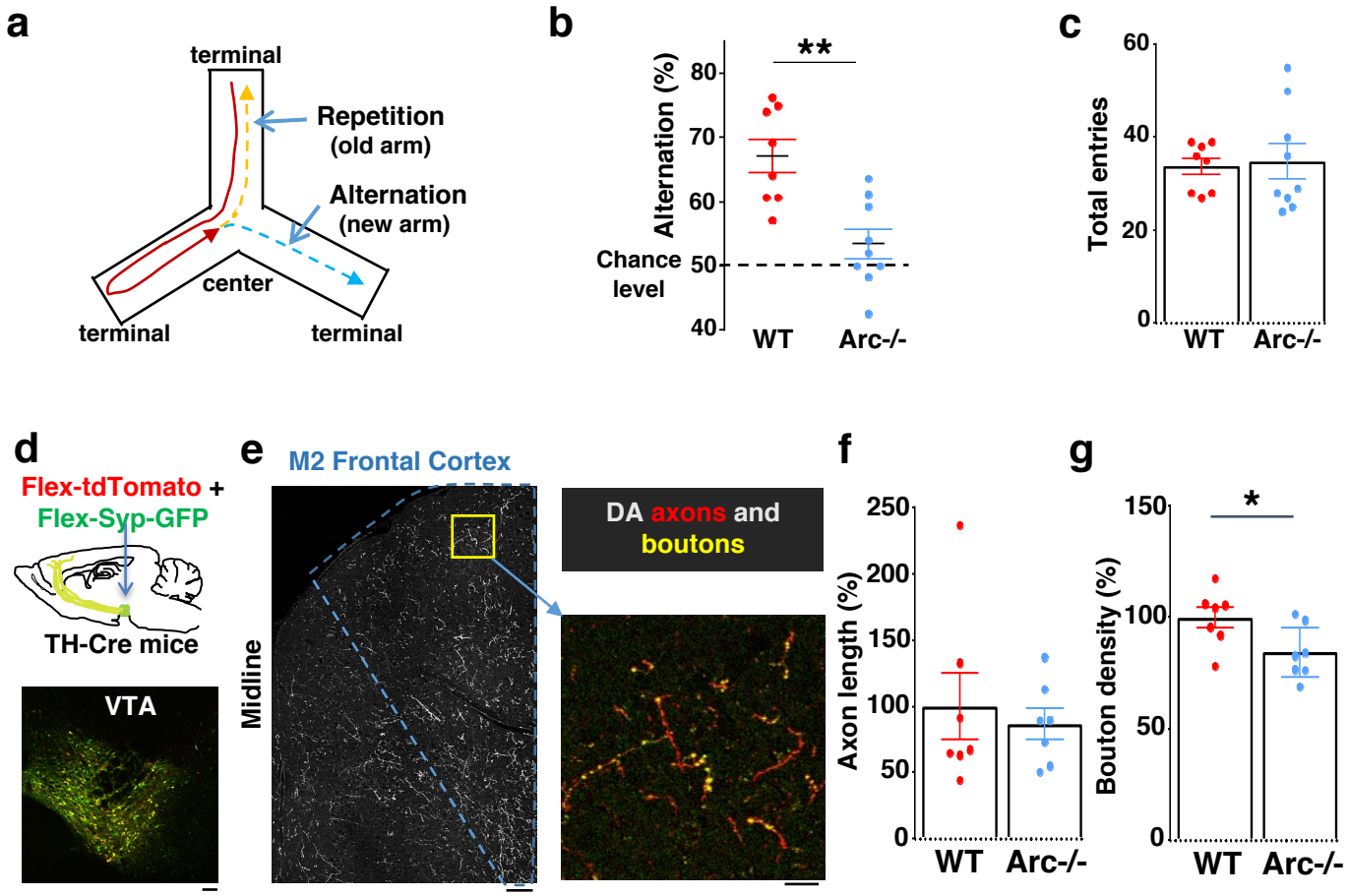
a
terminal
Repetition
(old arm)
Alternation
(new arm)
center
terminal
terminal
b
**
Alternation (%)
80
70
60
Chance
level
50
40
WT
Arc-/-
c
Total entries
60
40
20
0
WT
Arc-/-
d
Flex-tdTomato +
Flex-Syp-GFP
TH-Cre mice
VTA
e
M2 Frontal Cortex
Midline
DA axons and
boutons
f
Axon length (%)
250
200
150
100
50
0
WT
Arc-/-
g
*
Bouton density (%)
150
100
50
0
WT
Arc-/-

Figure 1

Figure 1. Characterization of cognitive and mesofrontal deficits in *Arc* mutant mice.

(**a**) Diagram showing the navigation choices for mice in a Y-maze**.** At the center of the maze, a mouse has a choice to enter either a new arm (alternation) or a previously visited old arm. (**b**) Alternation percentage in the Y-maze task showing significant reduction in the *Arc*-/- animals compared to wildtype animals (**p=0.001, *t*-test, t(15)=3.975, *WT* N = 8, *Arc*-/- N = 9 mice). (**c**) Total arm entries are comparable between *Arc*-/- and *WT*. (**d**) Top**,** schematic for AAV injection in *TH-Cre* animals to label dopaminergic neurons. Bottom, confocal image showing tdTomato (red) and SypGFP (green) labeling in the VTA. Scale bar, 100 μm. (**e**) Left, confocal image showing labeled dopaminergic axons in the frontal cortex. The dotted line indicates the region-of-interest for M2. Scale bar, 100 μm. Right, zoomed-in region showing labeled axons (tdTomato, red) and boutons (tdTomato+SypGFP, yellow). Scale bar, 20 μm. (**f, g**) The normalized axon length (**f**) is not significantly different. The normalized bouton density (g) is significantly reduced in *Arc*-/- animals compared to *WT* (*p=0.034, *t*-test, t-test, t(12)=2.393, N=7 mice for each group). The axon length is normalized by the number of labeled cells in VTA, the bouton density is normalized by the axon length, and both are expressed as a percentage of the group average in *WT* mice. All the error bars indicate SEM.

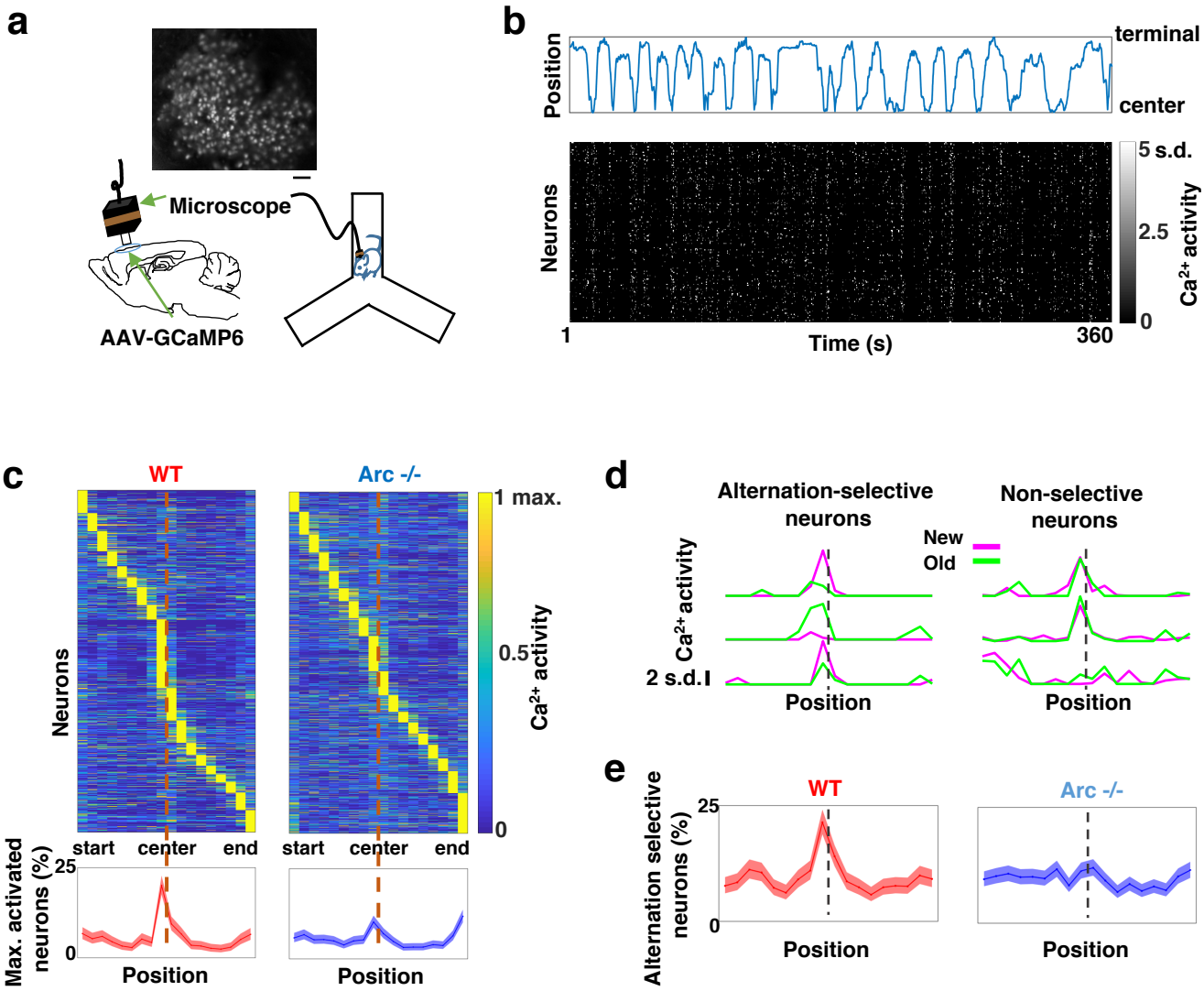
a
Microscope
AAV-GCaMP6
b
Position
terminal
center
Neurons
5 s.d.
2.5
0
Ca2+ activity
1
Time (s)
360
c
WT
Arc -/-
1 max.
0.5
0
Neurons
Ca2+ activity
start
center
end
start
center
end
Max. activated neurons (%)
25
0
Position
Position
d
Alternation-selective neurons
Non-selective neurons
New
Old
Ca2+ activity
2 s.d.
Position
Position
e
WT
Arc -/-
Alternation selective neurons (%)
25
0
Position
Position

Figure 2

Figure 2. Task-coordinated frontal neuronal ensemble activity is disrupted in *Arc* mutant mice.

(**a**) Diagram showing the setup for miniaturized microscope imaging of frontal cortical activity in mice performing the Y-maze task. The example image represents the projection (by standard deviation of ΔF/F) of a calcium activity movie (~500 s), showing labeled M2 frontal cortical neurons. Scale bar, 100 μm. (**b**) Top, an example plot showing the positions of a wildtype mouse relative to the Y-maze center during navigation. Bottom, raster plot showing the calcium activity of M2 neurons simultaneously recorded during navigation. (**c**) Top, the average activity of individual frontal cortical neurons at binned positions relative to the center of Y-maze in *WT* (938 neurons from 8 animals) and *Arc*-/- (1338 neurons from 7 animals) animals. Bottom, the proportion of neurons showing maximal activation at each maze position. This proportion peaked right before the maze center in *WT* mice but reduced significantly in *Arc*-/- mice. Shaded areas indicate 95% confidence intervals. (**d**) Examples of neurons showing differential (alternation-selective, traces from three neurons on the left) or similar (non-selective, traces from three neurons on the right) activity between new and old arm visits. (**e**) The proportion of alternation-selective neurons peaked right before the maze center in *WT* mice but reduced significantly in *Arc*-/- mice. Shaded areas indicate 95% confidence intervals.

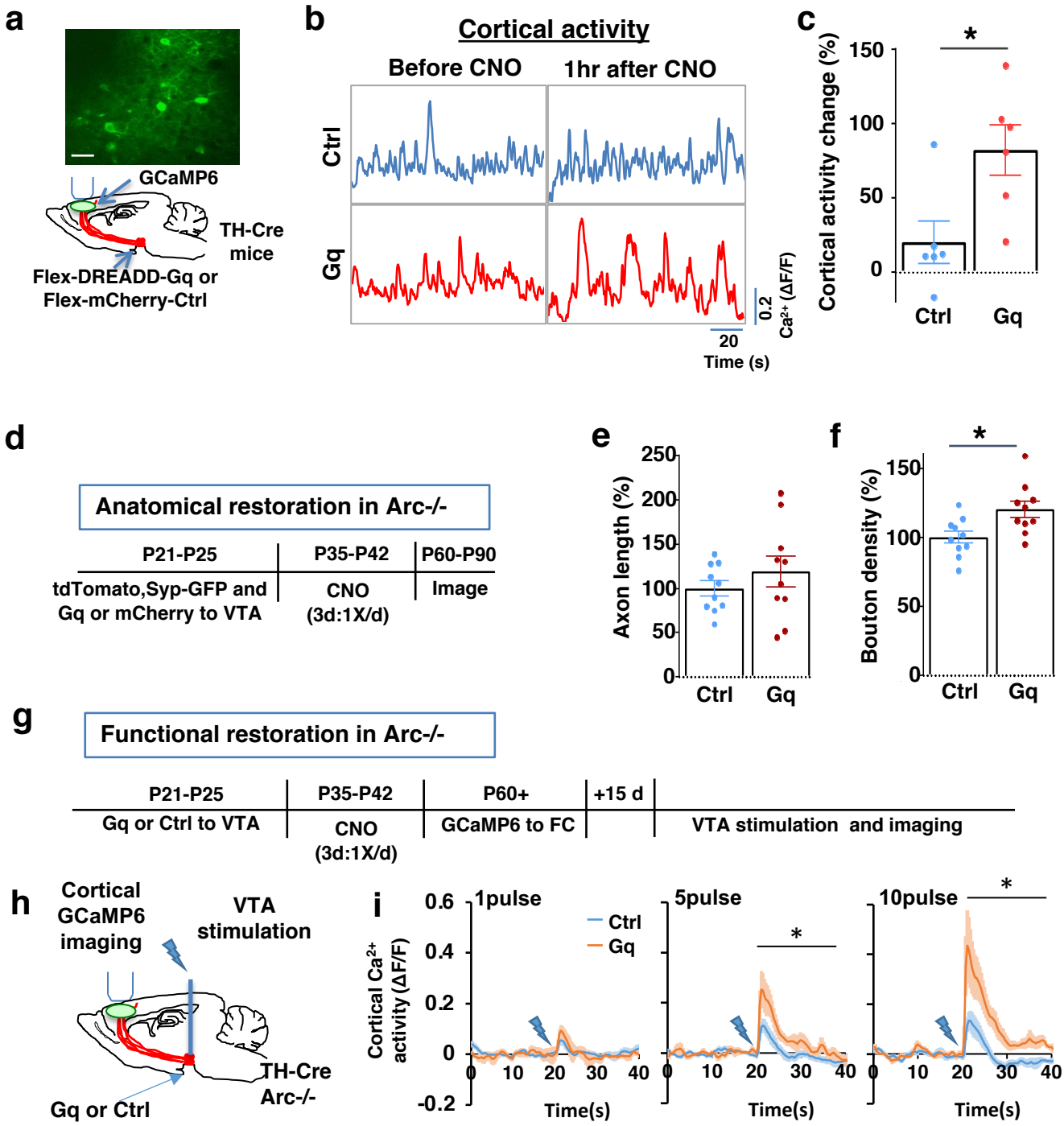
a
GCaMP6
TH-Cre mice
Flex-DREADD-Gq or Flex-mCherry-Ctrl
b
Cortical activity
Before CNO
1hr after CNO
Ctrl
Gq
0.2
Ca2+ (ΔF/F)
20
Time (s)
c
Cortical activity change (%)
150
100
50
0
*
Ctrl
Gq
d
Anatomical restoration in Arc-/-
P21-P25
P35-P42
P60-P90
tdTomato,Syp-GFP and Gq or mCherry to VTA
CNO (3d:1X/d)
Image
e
Axon length (%)
250
200
150
100
50
0
Ctrl
Gq
f
Bouton density (%)
150
100
50
0
*
Ctrl
Gq
g
Functional restoration in Arc-/-
P21-P25
P35-P42
P60+
+15 d
Gq or Ctrl to VTA
CNO (3d:1X/d)
GCaMP6 to FC
VTA stimulation and imaging
h
Cortical GCaMP6 imaging
VTA stimulation
TH-Cre Arc-/-
Gq or Ctrl
i
Cortical Ca2+ activity (ΔF/F)
0.6
0.4
0.2
0
-0.2
1pulse
5pulse
10pulse
Ctrl
Gq
*
*
0
10
20
30
40
Time(s)

Figure 3

Figure 3. Adolescent dopamine neuron stimulation leads to long-term reversal of mesofrontal circuit deficits.

(**a**) Schematic for labeling dopamine neurons with DREADD-Gq-mCherry and imaging frontal cortical activity with GCaMP6. The example image at the top shows a two-photon image of labeled cortical neurons. Scale bar, 20 μm. (**b**) Example traces of spontaneous cortical activity averaged from the whole image frame in control mCherry only (blue) and DREADD-Gq (red) animals before and 1hr after CNO injection. (**c**) Gq animals show significantly higher change in cortical activity after CNO injection compared to control mCherry only animals, suggesting CNO-induced activation of the mesofrontal circuit (*p=0.018, *t*-test, t(10)=2.814, N=6 mice for each group). Cortical activity is summarized by the standard deviation (SD) of the spontaneous activity traces. Activity change is calculated as (SD2-SD1)/SD1, where SD1 is before and SD2 after treatment. (**d**) Diagram showing experimental procedures to evaluate the effect of adolescent dopamine neuron stimulation on the structure of frontal dopaminergic projections. (**e, f**) Normalized axon length (**e**) is not significantly different. Normalized bouton density (**f**) is significantly increased in Gq animals compared to Ctrl (*p=0.013, *t*-test, t(18)=2.763, N = 10 for each group). The axon length is normalized by the number of labeled cells in VTA, the bouton density is normalized by the axon length, and both are expressed as a percentage of the group average in Ctrl mice. (**g**) Diagram showing procedures to determine the effect of adolescent dopamine neuron stimulation on mesofrontal circuit activity in *Arc*-/-;*TH-Cre* mice labeled with DREADD-Gq or mCherry-Ctrl. (**h**) Schematic showing the experimental setup to measure the mesofrontal circuit activity by VTA electrical stimulation and GCaMP6 imaging in the frontal cortex. (**i**) Time courses of cortical calcium signals in response to VTA stimulation in *Arc*-/-;mCherry-Ctrl and *Arc*-/-; DREADD-Gq mice. 1, 5, or 10 pulses of electrical stimuli (50 Hz) was delivered at 20 seconds after the start of

imaging. The cortical calcium activity at each time point is represented by the change in image fluorescence relative to the baseline image fluorescence ($\Delta F/F$). (5 pulse $F(1,10)=6.0$, $^*p=0.034$, 10 pulse $F(1,10)=9.5$, $^*p=0.012$, Two-way ANOVA, N=6 mice per group).

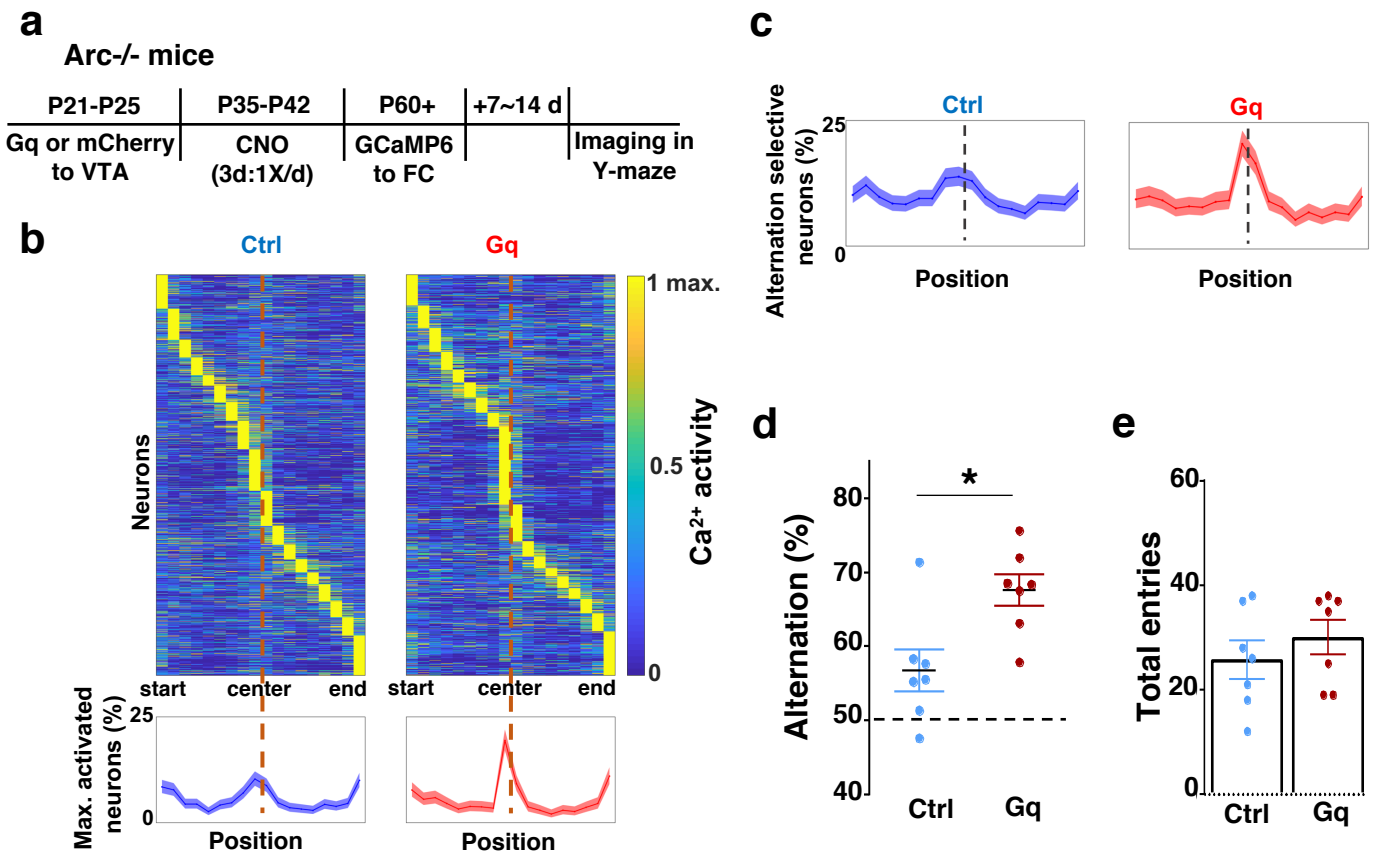
a
Arc-/- mice
P21-P25
P35-P42
P60+
+7~14 d
Gq or mCherry to VTA
CNO (3d:1X/d)
GCaMP6 to FC
Imaging in Y-maze
b
Ctrl
Gq
1 max.
0.5
0
Ca2+ activity
Neurons
start
center
end
Max. activated neurons (%)
25
0
Position
c
Alternation selective neurons (%)
Ctrl
Gq
25
0
Position
d
Alternation (%)
80
70
60
50
40
*
Ctrl
Gq
e
Total entries
60
40
20
0
Ctrl
Gq

Figure 4

Figure 4. Adolescent dopamine neuron stimulation leads to restoration of coordinated frontal neuronal activity and cognition in adulthood.

(**a**) Diagram showing procedures for adolescent stimulation of dopamine neurons and functional imaging of frontal cortical neuron activity in adult *Arc*-/-;*TH-Cre* mice. (**b**) The average activity of individual frontal cortical neurons at binned positions relative to the center of Y-maze in *Arc* -/-; mCherry-Ctrl (1288 neurons from 7 mice) and *Arc*-/-; DREADD-Gq (1008 neurons from 7 mice) animals. Bottom, the proportion of neurons showing maximal activation at each maze position. This proportion reached a higher peak right before the maze center in *Arc*-/-; DREADD-Gq mice compared to *Arc*-/-; mCherry-Ctrl mice. Shaded areas indicate 95% confidence intervals. (**c**) The proportion of alternation-selective neurons reached a significantly higher peak right before the maze center in *Arc*-/-; DREADD-Gq compared to *Arc*-/-; mCherry-Ctrl mice. Shaded areas indicate 95% confidence intervals. (**d**) Y-maze alternation percentage for the animals used in the miniaturized microscope imaging experiments shows significant increase in *Arc*-/-;DREADD-Gq animals compared to *Arc*-/-; mCherry-Ctrl (*p=0.010, *t*-test, t-test, t(12)=3.043, N = 7 mice for each group). (**e**) Total arm entries are not significantly different (p=0.399, *t*-test, t(12)=0.875). All the error bars indicate SEM.

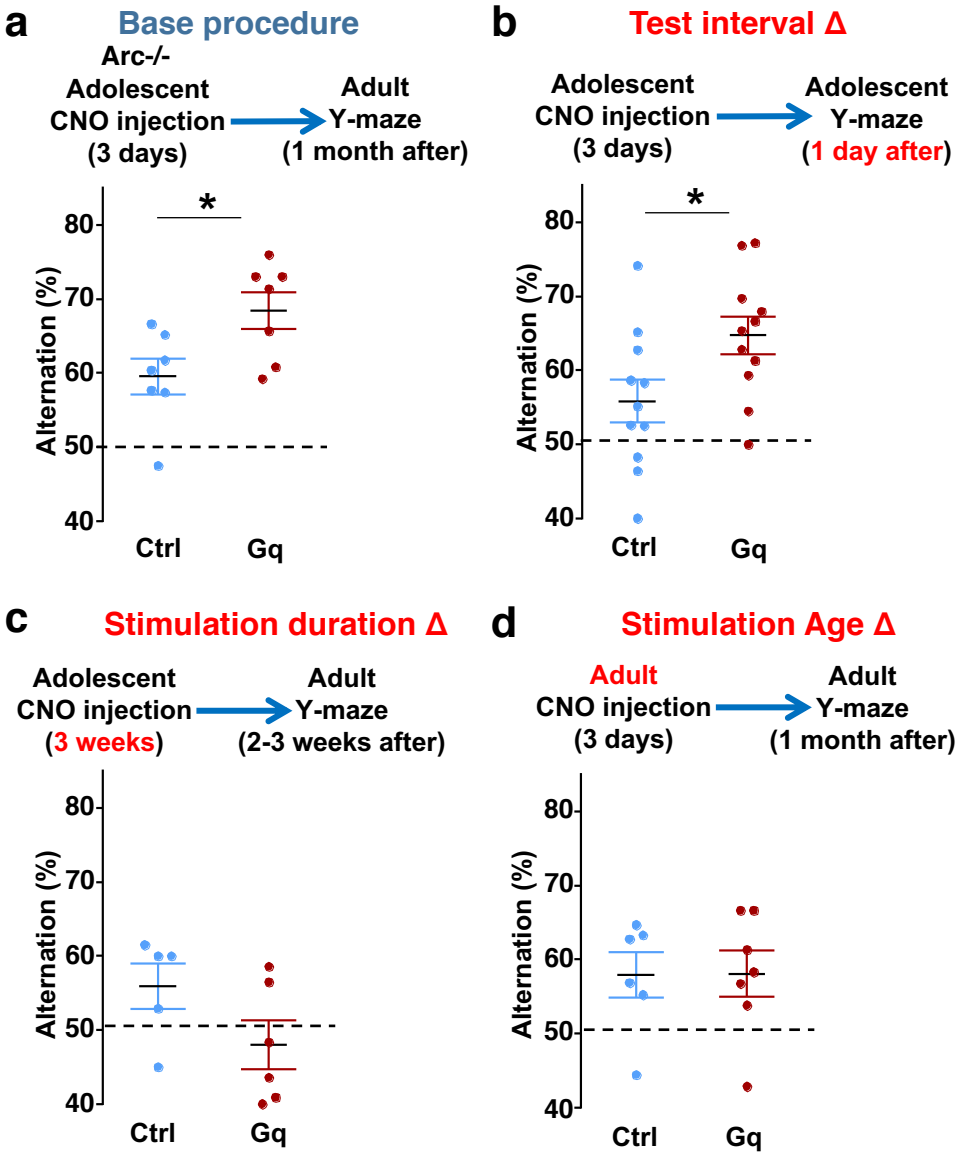
a
Base procedure
Arc-/-
Adolescent
CNO injection
(3 days)
Adult
Y-maze
(1 month after)
*
Alternation (%)
80
70
60
50
40
Ctrl
Gq
b
Test interval Δ
Adolescent
CNO injection
(3 days)
Adolescent
Y-maze
(1 day after)
*
Alternation (%)
80
70
60
50
40
Ctrl
Gq
c
Stimulation duration Δ
Adolescent
CNO injection
(3 weeks)
Adult
Y-maze
(2-3 weeks after)
Alternation (%)
80
70
60
50
40
Ctrl
Gq
d
Stimulation Age Δ
Adult
CNO injection
(3 days)
Adult
Y-maze
(1 month after)
Alternation (%)
80
70
60
50
40
Ctrl
Gq

Figure 5

Figure 5. Efficacy requirements for adolescent dopamine neuron stimulation.

(**a**) Top, diagram showing the base procedure for the stimulation of midbrain dopamine neurons and Y-maze testing in *Arc*-/-;*TH-Cre* mice labeled with DREADD-Gq or mCherry control viruses. Animals were injected with CNO (1 mg/kg) once per day for 3 days in adolescence (5 weeks old) and then tested in the Y-maze at adulthood (~1 month later). *Arc*-/-; DREADD-Gq animals show significantly higher alternation compared to *Arc*-/-; mCherry-Ctrl at adulthood (*p=0.023, *t*-test, t(12)=2.598, N=7 mice for each group). (**b**) The behavioral effect at the test interval of 1 day after CNO injection. *Arc*-/-; DREADD-Gq animals show significantly higher alternation compared to *Arc*-/-; mCherry-Ctrl (*p=0.031, *t*-test, t(20)=2.322, N=11 mice for each group). (**c**) The behavioral outcome following a long duration stimulation starting in adolescence (2 times per day, 5 days per week, for 3 weeks). These animals did not show any improvement but a declining trend in performance (p=0.12, *t*-test, t(9)=1.727, *Arc*-/-; mCherry-Ctrl N=5, *Arc*-/-; DREADD-Gq, N=6 mice). (**d**) The behavioral outcome following three days of CNO stimulation administered in adult mice (2-3 months). These animals did not show significant difference (p=0.97, *t*-test, t(11)=0.037, *Arc*-/-;mCherry-Ctrl, N=6; *Arc*-/-;DREADD-Gq, N=7 mice).

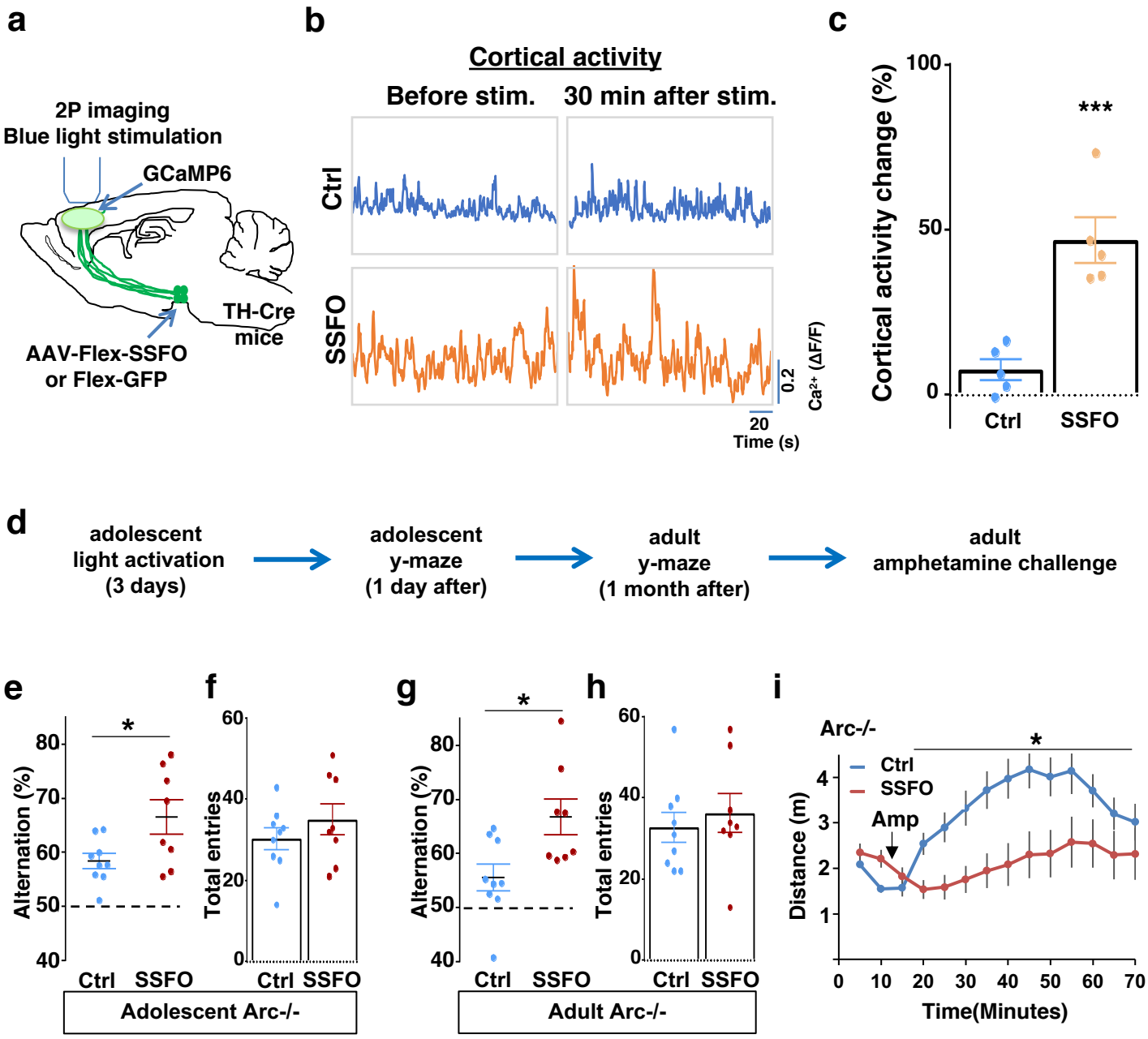
a
2P imaging
Blue light stimulation
GCaMP6
TH-Cre mice
AAV-Flex-SSFO or Flex-GFP
b
Cortical activity
Before stim.
30 min after stim.
Ctrl
SSFO
0.2
Ca2+ (ΔF/F)
20
Time (s)
c
Cortical activity change (%)
100
50
0
***
Ctrl
SSFO
d
adolescent light activation (3 days)
adolescent y-maze (1 day after)
adult y-maze (1 month after)
adult amphetamine challenge
e
Alternation (%)
*
Ctrl
SSFO
f
Total entries
Ctrl
SSFO
Adolescent Arc-/-
g
Alternation (%)
*
Ctrl
SSFO
h
Total entries
Ctrl
SSFO
Adult Arc-/-
i
Arc-/-
Ctrl
SSFO
Amp
*
Distance (m)
Time(Minutes)

Figure 6

Figure 6. Specific stimulation of adolescent frontal dopaminergic axons leads to reversal of both cognitive and psychomotor deficits.

(**a**) Schematic for labeling dopamine neurons with SSFO and two-photon imaging of frontal cortical activity with GCaMP6. (**b**) Example traces of spontaneous cortical activity averaged from the whole image frame in control EGFP only (blue) and SSFO (orange) labeled animals before and 30 min after frontal cortical blue light stimulation. (**c**) SSFO animals show significantly higher change in cortical activity (summarized by the standard deviation of spontaneous activity traces) compared to control EGFP animals after the light activation, suggesting light activation of SSFO expressing dopamine neurons (*p=0.001, *t*-test, t(8)=5.135, N=5 mice for each group). Cortical activity is summarized by the standard deviation (SD) of the spontaneous activity traces. Activity change is calculated as (SD2-SD1)/SD1, where SD1 is before and SD2 after treatment. (**d**) Diagram showing procedures for local light activation of frontal dopaminergic projections and Y-maze testing in *Arc-/-;TH-Cre* mice labeled with SSFO or Ctrl-GFP viruses. Light activation was delivered in adolescence (5 weeks old) once per day for 3 days. Animals were first tested in the Y-maze 1 day after the last light activation and then tested again in the Y-maze at adulthood, followed by an amphetamine induced locomotion test. (**e-h**) SSFO expressing animals show significantly higher alternation compared to control animals 1 day after light activation **e**, (*p=0.028, *t*-test, t(15)=2.440, N=9 EGFP, N=8 SSFO mice), with no difference in total entries **f**. These animals also show higher alternation at adulthood **g**, (*p=0.015, *t*-test, t(15)=2.748, EGFP N=9, SSFO N=8) with no difference in total entries **h**. (**i**) In *Arc-/-;TH-Cre* mice that received adolescent frontal light stimulation, amphetamine induced locomotion is significantly reduced at adulthood in SSFO animals compared to GFP-control animals (F(1,14)=5.3, *p=0.037, Two-way ANOVA, N=8 mice per group). All the error bars indicate SEM.

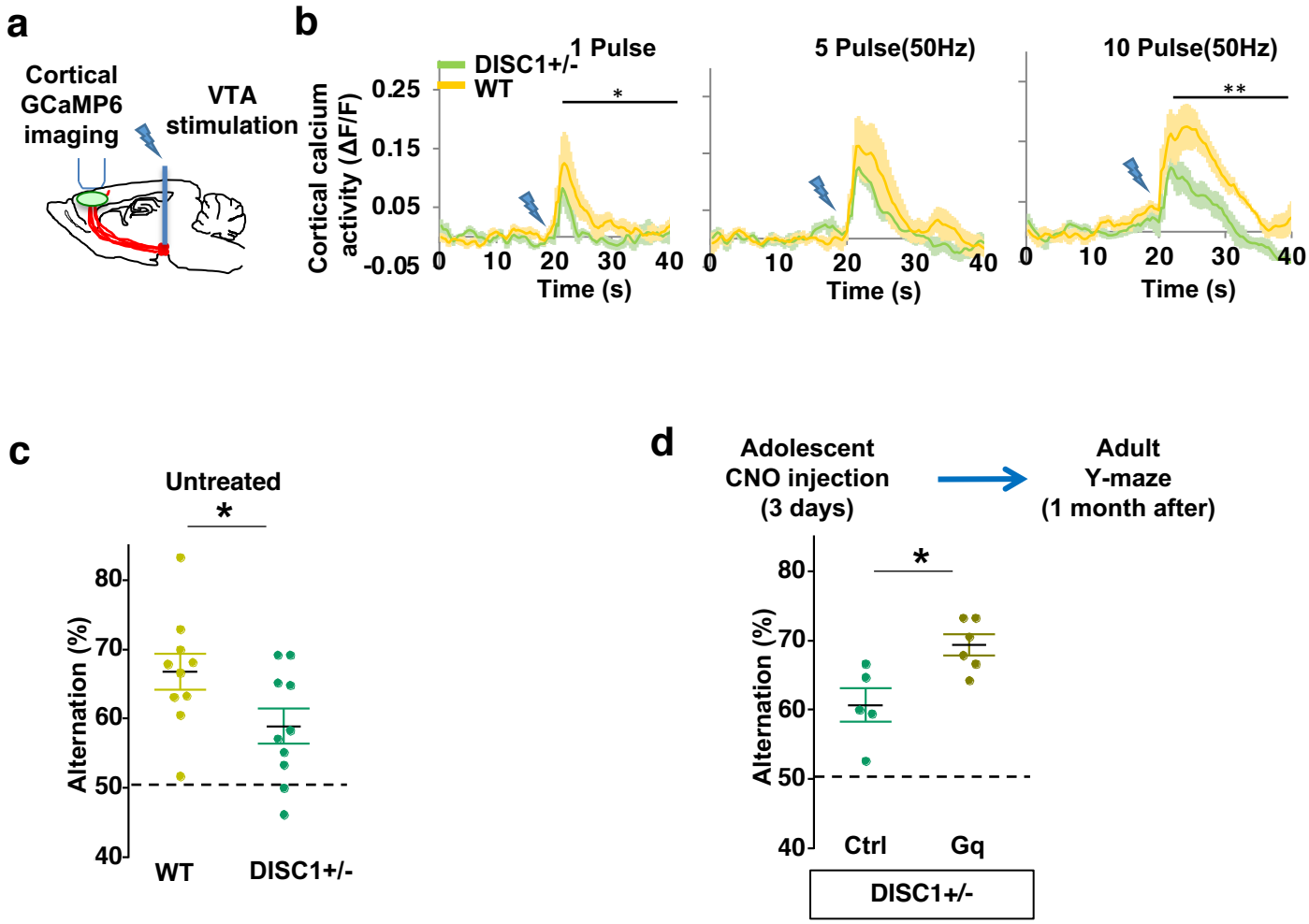
a
Cortical GCaMP6 imaging
VTA stimulation
b
DISC1+/-
WT
1 Pulse
5 Pulse(50Hz)
10 Pulse(50Hz)
Cortical calcium activity (ΔF/F)
0.25
0.15
0.05
-0.05
*
**
0
10
20
30
40
Time (s)
c
Untreated
*
Alternation (%)
80
70
60
50
40
WT
DISC1+/-
d
Adolescent CNO injection (3 days)
Adult Y-maze (1 month after)
*
Alternation (%)
80
70
60
50
40
Ctrl
Gq
DISC1+/-

Figure 7

Figure 7. Adolescent dopamine neuron stimulation reverses cognitive deficits in *DISC1* mutant mice.

(**a**) Schematic showing the experimental setup to measure the mesofrontal circuit activity by VTA electrical stimulation and GCaMP6 imaging in the frontal cortex. (**b**) Time courses of cortical calcium signals in response to VTA stimulation in *WT and DISC1*+/- mice. 1, 5, or 10 pulses of electrical stimuli (50 Hz) was delivered at 20 seconds after the start of imaging. The cortical calcium activity at each time point is represented by the change in image fluorescence relative to the baseline image fluorescence (ΔF/F). (1 pulse F(1,10)=5.7, *p=0.038; 10 pulse F(1,10)=16.5, *p=0.002, Two-way ANOVA, N=6 per group). (**c**) *DISC1*+/- mice shows significant reduction in Y-maze alternation compared to *WT* (*p=0.044, *t*-test, t(18)=2.171, N=10 mice for each group). (**d**) *DISC1*+/-;*TH-Cre* mice with DREADD-Gq labeled dopamine neurons show significantly higher alternation in the Y-maze at adulthood compared to mCherry-Ctrl labeled mice after 3-day adolescent CNO injections (*p=0.012, *t*-test, t(9)=3.139, *DISC1*+/-; mCherry N = 5, *DISC1*+/-;DREADD-Gq, N=6 mice). All the error bars indicate SEM.